

## DYNAMICS OF LUMINOUS GALAXIES. II. SURFACE PHOTOMETRY AND VELOCITY DISPERSIONS OF BRIGHTEST CLUSTER MEMBERS

ELIOT M. MALUMUTH<sup>1</sup> AND ROBERT P. KIRSHNER<sup>1,2</sup>

Department of Astronomy, University of Michigan

Received 1983 September 9; accepted 1984 October 8

### ABSTRACT

Velocity dispersions for 46 galaxies and CCD surface photometry for 27 galaxies have been obtained using the McGraw-Hill Observatory 1.3 m and the KPNO No. 1 0.9 m telescopes. The results provide a greatly improved set of data for investigating the brightest galaxies in galaxy clusters. We find that the brightest cluster members (BCMs) are substantially brighter than predicted from their velocity dispersions and the  $L \propto \sigma^4$  relation for elliptical galaxies. In the range of velocity dispersion from 193 to 346 km s<sup>-1</sup>, the BCMs average 1.22 mag brighter than E galaxies. We consider the possibility that this might be a selection effect due to the spread of  $M$  at given  $\sigma$ , but show that the observed distribution of luminosity excess does not correspond to a simple model of selection unless the elliptical galaxy sample suffers a Malmquist bias of 0.4 mag. We note that our data show that the BCMs with the largest excess luminosity have the largest effective radii and the lowest surface brightnesses, as predicted by homologous merger models. One result that is not predicted by simple merger models is that the surface brightness profiles of the galaxies which have the largest excess luminosities are the flattest. Another is that the  $V$  band mass-to-light ratios for BCM galaxies in this sample average  $9.0 \pm 0.8$ , as compared with  $6.5 \pm 0.7$  for our elliptical galaxies.

*Subject headings:* galaxies: clustering — galaxies: internal motions — galaxies: photometry

### I. INTRODUCTION

The dynamical and photometric properties of cD galaxies may provide important clues to understanding their origin and evolution. Whether cD's are just the largest elliptical galaxies (Peebles 1968; Geller and Peebles 1976), or are produced by special dynamical processes that alter galaxies in clusters where the cD galaxies are found (Peach 1969; Sandage 1976; Tremaine and Richstone 1977; Ostriker and Hausman 1977, hereafter OH; Hausman and Ostriker 1978, hereafter HO), should leave a signature in the present properties of the cD galaxies. Since these galaxies are among the brightest objects in the universe, there are strong reasons to use them as standard candles in cosmology, but first it is essential to understand their photometric properties and the variation of those properties (Gunn and Oke 1975; Sandage, Kristian, and Westphal 1976). To gain a deeper understanding of these galaxies, we presented in Paper I (Malumuth and Kirshner 1981) velocity dispersions for eight brightest cluster member (BCM) galaxies for which Oemler (1976, hereafter O76) had published surface brightness profiles. In this paper new spectroscopic and photometric observations are used to increase the number of BCM galaxies with both velocity dispersions and surface photometry to 31.

Although the sample in Paper I was quite small, there were several tantalizing results. One was that the  $L \propto \sigma^4$  relation for elliptical galaxies (Faber and Jackson 1976; Sargent *et al.* 1977; Schechter and Gunn 1979; and Schechter 1980) predicts the luminosity of the BCM galaxies poorly. The BCM galaxies averaged 0.5 mag brighter than elliptical galaxies at the same velocity dispersion. The core radius and effective surface brightness were correlated with the luminosity difference in the

sense that galaxies with large positive residuals were physically larger and had lower surface brightness than those with small residuals.

While these results are not by themselves inconsistent with the idea that BCM galaxies are drawn from the same luminosity function as the elliptical galaxies (Peebles 1968; Geller and Peebles 1976), they are in good accord with predictions of the contrasting idea present in the simple homologous merger models of OH and HO. In these models, each merger results in a brighter galaxy than the initial galaxy, but the velocity dispersion does not change. The luminosity residual would be a measure of the amount of evolution that a given BCM has undergone. The correlation of  $R_c$  and  $I_e$  with that residual is consistent with the dynamical evolution picture of cD galaxy formation. However, the small average value of the residual and the small number of galaxies weaken the result. This paper improves that situation by substantially extending the sample. We obtained spectra of 46 BCM galaxies and analyzed them using the Fourier quotient method (Sargent *et al.* 1977) to determine velocity dispersions. We also obtained CCD photometry to measure the surface brightness profiles of 27 BCM galaxies. These new data are then examined in the light of the results of Paper I.

We present the velocity dispersion measurements in § II, and the surface photometry measurements in § III. In § IV we discuss the positions of the BCM galaxies in the  $L$ - $\sigma$  plane in terms of the merger hypothesis of cD formation. The results are summarized in § V.

### II. VELOCITY DISPERSIONS

#### a) *The Sample*

Our aim is to compare the dynamical and photometric properties of cD galaxies to those of bright elliptical galaxies. We obtained velocity dispersions for 28 BCM galaxies in Abell (1958) rich clusters, 13 BCMs in "poor clusters" (Morgan, Kayser, and White 1975, hereafter MKW; Albert, White, and

<sup>1</sup> Guest observers, Kitt Peak National Observatory, which is operated by the Association of Universities for Research in Astronomy, Inc., under contract with the National Science Foundation.

<sup>2</sup> Alfred P. Sloan Foundation Research Fellow.

Morgan 1977, hereafter AWM) and five BCM galaxies in other groups or clusters. Eight of these galaxies were chosen because photometry that extended to faint surface brightness limits was available (O76). The rest of the BCM galaxies were chosen on the basis of Bautz-Morgan type, since the original definition of the Bautz-Morgan type I cluster was that it contained a single dominant cD galaxy (Bautz and Morgan 1970). The classification scheme proceeds through types I-II, II, II-III, and III in order of decreasing dominance of the BCM galaxy. Most of the BCM galaxies in this sample are in Bautz-Morgan type I or type I-II clusters (21 of the 28 Abell clusters). The sample also emphasizes low-redshift galaxies, since more distant galaxies would have taken prohibitively long to observe with the McGraw-Hill Observatory 1.3 m telescope. All of the observed galaxies have redshifts less than  $z = 0.08$ , with a mean of

$z = 0.035$ . Galaxies with multiple nuclei were generally avoided because of the possibility of confusion over which of the nuclei is the dynamical center of the cD galaxy. The multiple nucleus galaxies A2199 and A2634 were observed because they had surface photometry from O76. In both cases the largest nucleus was taken to be the center of the cD galaxy. In the case of A2634 both nuclei were observed: the southern one was the larger of the two. Since the difference in redshift between the two nuclei is  $990 \text{ km s}^{-1}$ , it seems likely that the northern one is just a small galaxy in the line of sight.

Thirty-one other galaxies were observed, most of which are elliptical galaxies, but some of which may be S0 galaxies. These galaxies are typically second or lower ranked members of various nearby clusters. All of the galaxies observed for velocity dispersion are listed in Table 1, along with the Bautz-

TABLE 1  
VELOCITY DISPERSIONS

Galaxy	Cluster	Bautz-Morgan Type	Richness	Counts ( $10^5$ )	$\sigma$	$z$	Run
BCM Galaxies							
...	A76	II-III	0	4	$236 \pm 24$	0.0383	1980 Sep
...	A119	II-III	1	4	$306 \pm 31$	0.0451	1980 Sep
...	A150	I-II	1	4	$245 \pm 35$	0.0599	1979 Nov
...	A151	II	1	4	$330 \pm 31$	0.0532	1980 Sep
...	A194	II	0	4	$246 \pm 23$	0.0181	1980 Sep
...	A261	I	1	4	$408 \pm 33$	0.0467	1979 Nov
...	A401	I	2	3	$367 \pm 35$	0.0744	1979 Nov
...	A496	I	1	4	$254 \pm 27$	0.0325	1979 Nov
...	A505	I	0	4	$408 \pm 43$	0.0540	1979 Nov
...	A754	I-II	2	4	$353 \pm 32$	0.0539	1979 Nov
NGC 2831	A779	I-II	0	5	$372 \pm 26$	0.0234	1979 May
...	A957	I-II	1	4	$311 \pm 29$	0.0443	1979 Nov
...	A994	I	1	4	$330 \pm 28$	0.0390	1979 Nov
...	A1177	I	0	4	$279 \pm 16$	0.0319	1980 Feb
...	A1631	I	0	5	$249 \pm 26$	0.0128	1979 May
...	A1775	I	2	4	$321 \pm 35$	0.0689	1980 Feb
...	A2052	I-II	0	3	$197 \pm 36$	0.0348	1979 May
...	A2107	I	1	3	$438 \pm 54$	0.0425	1980 Sep
...	A2147	III	1	5	$306 \pm 42$	0.0357	1979 May
NGC 6086	A2162 <sup>a</sup>	II-III	0	6	$342 \pm 26$	0.0321	1979 May
NGC 6166	A2199	I	2	4	$439 \pm 46$	0.0309	1980 Sep
...	A2366	I-II	0	4	$391 \pm 35$	0.0542	1979 Nov
...	A2457	I-II	1	3	$477 \pm 41$	0.0595	1979 Nov
...	A2589 <sup>a</sup>	I	1	4	$346 \pm 27$	0.0420	1979 Nov
NGC 7720N } NGC 7720S }	A2634	II	1	4	$215 \pm 25$	0.0276	1979 Nov
NGC 7768	A2666	I	0	4	$363 \pm 30$	0.0278	1979 Nov
...	A2670	I-II	3	4	$426 \pm 42$	0.0776	1979 Nov
NGC 3090	MKW 1 <sup>b</sup>	II-III	-2	4	$255 \pm 22$	0.0202	1979 Nov
...	MKW 2 <sup>b</sup>	I	0	4	$416 \pm 30$	0.0383	1979 Nov
NGC 4073	MKW 4 <sup>b</sup>	I	-1	6	$243 \pm 23$	0.0192	1979 May
NGC 5400	MKW 5 <sup>b</sup>	I	-3	5	$364 \pm 52$	0.0253	1979 May
...	MKW 1s <sup>b</sup>	I	-3	4	$206 \pm 19$	0.0168	1979 Nov
...	MKW 2s <sup>b</sup>	II-III	-1	3	$301 \pm 29$	0.0302	1979 Nov
NGC 2804	AWM 1 <sup>b</sup>	II-III	-1	5	$206 \pm 19$	0.0271	1979 May
NGC 4213	AWM 2 <sup>b</sup>	I-II	-2	6	$247 \pm 28$	0.0223	1979 May
NGC 5629	AWM 3 <sup>b</sup>	II	-2	6	$328 \pm 29$	0.0152	1979 May
...	AWM 4 <sup>b</sup>	I	-1	4	$278 \pm 40$	0.0325	1981 Apr
NGC 6269	AWM 5 <sup>b</sup>	I-II	-1	4	$228 \pm 24$	0.0356	1980 Sep
IC 4062	AWM 6 <sup>b</sup>	I	-2	5	$327 \pm 27$	0.0357	1979 May
NGC 1129	AWM 7 <sup>b</sup>	I	0	4	$335 \pm 25$	0.0182	1979 Nov
NGC 741	NGC 741 <sup>a</sup>	II	0	4	$345 \pm 28$	0.0189	1979 Nov
NGC 1600	NGC 1600 <sup>a</sup>	I	0	4	$363 \pm 28$	0.0154	1979 Nov
NGC 3158	NGC 3158 <sup>a</sup>	I-II	0	4	$390 \pm 30$	0.0224	1979 Nov
NGC 4486	Virgo <sup>a</sup>	III	1	5	$318 \pm 46$	0.0038	1979 May
NGC 4486	Virgo <sup>a</sup>	III	1	6	$411 \pm 43$	0.0045	1981 Feb
NGC 4486	Virgo <sup>a</sup>	III	1	7	$302 \pm 33$	0.0040	1981 Apr
NGC 4889	Coma <sup>a</sup>	II	2	5	$428 \pm 31$	0.0214	1980 Feb
NGC 7619	Pegasus 1 <sup>a</sup>	II	0	5	$336 \pm 23$	0.0133	1979 Nov

TABLE 1—Continued

Galaxy	Cluster	Bautz-Morgan Type	Richness	Counts ( $10^5$ )	$\sigma$	$z$	Run
Elliptical Galaxies							
NGC 533	...	...	...	4	$284 \pm 35$	0.0189	1979 Nov
NGC 636	...	...	...	6	$174 \pm 17$	0.0064	1980 Sep
NGC 1052	...	...	...	5	$192 \pm 33$	0.0052	1980 Sep
NGC 1209	...	...	...	4	$281 \pm 21$	0.0088	1979 Nov
NGC 1272	Perseus <sup>a</sup>	II-III	2	4	$344 \pm 23$	0.0131	1980 Feb
NGC 1273	Perseus <sup>a</sup>	II-III	2	4	$259 \pm 20$	0.0182	1980 Feb
NGC 1278	Perseus <sup>a</sup>	II-III	2	4	$245 \pm 28$	0.0205	1980 Feb
NGC 1316	Fornax <sup>a</sup>	II-III	1	8	$223 \pm 23$	0.0058	1980 Sep
NGC 1400	...	...	...	4	$250 \pm 29$	0.0017	1980 Sep
NGC 1426	...	...	...	4	$153 \pm 22$	0.0044	1980 Sep
NGC 1521	...	...	...	4	$296 \pm 27$	0.0135	1979 Nov
NGC 1700	...	...	...	5	$267 \pm 20$	0.0126	1979 Nov
NGC 1889	...	...	...	4	$90 \pm 20$	0.0079	1979 Nov
NGC 2629	...	...	...	5	$303 \pm 31$	0.0128	1979 Nov
NGC 2672	...	...	...	4	$332 \pm 24$	0.0140	1979 Nov
NGC 2693	...	...	...	4	$297 \pm 26$	0.0163	1979 Nov
NGC 2768	...	...	...	5	$207 \pm 23$	0.0049	1070 Nov
NGC 4374	Virgo <sup>a</sup>	III	1	7	$299 \pm 21$	0.0030	1979 May
NGC 4406	Virgo <sup>a</sup>	III	1	6	$244 \pm 19$	-0.0012	1979 May
NGC 4458	Virgo <sup>a</sup>	III	1	5	$176 \pm 21$	0.0021	1981 Apr
NGC 4467	Virgo <sup>a</sup>	III	1	4	$102 \pm 17$	0.0047	1981 Apr
NGC 4472	Virgo <sup>a</sup>	III	1	7	$343 \pm 20$	0.0027	1979 May
NGC 4472	Virgo <sup>a</sup>	III	1	6	$363 \pm 30$	0.0031	1981 Apr
NGC 4473	Virgo <sup>a</sup>	III	1	5	$203 \pm 12$	0.0071	1980 Feb
NGC 4564	Virgo <sup>a</sup>	III	1	7	$245 \pm 20$	0.0037	1981 Apr
NGC 4649	Virgo <sup>a</sup>	III	1	9	$324 \pm 25$	0.0034	1981 Feb
NGC 4692	Coma <sup>a</sup>	II	2	5	$230 \pm 27$	0.0267	1981 Feb
NGC 4874	Coma <sup>a</sup>	II	2	4	$311 \pm 29$	0.0241	1980 Feb
NGC 6703	...	...	...	5	$159 \pm 19$	0.0090	1980 Sep
NGC 7626	Pegasus I <sup>a</sup>	II	0	4	$310 \pm 23$	0.0119	1979 Nov
NGC 7626	Pegasus I <sup>a</sup>	II	0	4	$274 \pm 26$	0.0123	1980 Sep
IC 708	A1314	III	0	5	$283 \pm 25$	0.0317	1979 May

<sup>a</sup> Bautz-Morgan type and richness from Sandage and Hardy 1973.

<sup>b</sup> Bautz-Morgan type and richness from Bahcall 1980.

Morgan type and cluster richness for each cluster. The Bautz-Morgan types are from Leir and van den Bergh (1977) unless otherwise indicated.

#### b) Observations and Analysis

The spectroscopic observations were obtained with the 1.3 m telescope of the McGraw-Hill Observatory in six runs: 1979 May, 1979 November, 1980 February, 1980 September, 1981 February, and 1981 April. Some of the results from the 1979 May, 1979 November, 1980 February, and 1980 September runs were previously reported in Paper I. An intensified Reticon scanner with event-centering electronics was used to obtain data in 2048 data channels at a dispersion of  $1.1 \text{ \AA channel}^{-1}$ , and a full width at half-maximum resolution of about  $5 \text{ \AA}$ . In general a  $2.8 \times 10''$  slit was used for the 1979 May data and a  $4'' \times 10''$  slit was used for the other runs; however, the smaller slit was used for some of the fainter elliptical galaxies. While variations of velocity dispersion with radius are certainly possible, our evidence, based on a small sample of cD galaxies where we have spatially resolved velocity dispersion profiles, is that no significant systematic effect is introduced by the variation in projected slit size. The slit was aligned with the galaxy's minor axis in all cases. The central wavelength was  $5150 \text{ \AA}$  for the 1979 May run and  $4900 \text{ \AA}$  for all other runs. A minimum of  $2 \times 10^5$  counts was obtained for each galaxy, with  $4 \times 10^5$  counts in most cases. The number of counts obtained for each galaxy is listed in Table 1. The integration times varied from 10 minutes for NGC 4472 to 3.5

hours for the BCM galaxy in A401. Several late-type giant stars were obtained on each run, with the same instrumental setting as for the galaxies. These stars were typically G8 III-K5 III, and were used as templates in the Fourier quotient analysis. The stars usually had  $4 \times 10^6$  counts in their spectra.

The data were binned in steps in  $\log v$  which corresponded to  $46 \text{ km s}^{-1}$  from  $4150$  to  $5680 \text{ \AA}$ . A Fourier quotient method essentially identical with that of Sargent *et al.* (1977) was used to obtain the redshift  $z$ , the line-strength parameter  $\gamma$ , and the velocity dispersion  $\sigma$ . Corrections for the resolution width ( $W \approx 100 \text{ km s}^{-1}$ ) and drift in the wavelengths,  $D$ , were made as outlined by Whitmore, Kirshner, and Schechter (1979). The drift was determined by taking comparison spectra every hour or so and comparing the wavelengths obtained before and after a galaxy observation. The drift was typically smaller than  $35 \text{ km s}^{-1}$ ; however, it was considerably larger in a few cases (A194, A957, A2107, and A2199). The velocity dispersion and redshifts are given in columns (6) and (7) of Table 1. The redshifts have been corrected for galactic rotation using  $\Delta V = 300 \cos b \sin l$ . The errors in the redshifts were approximately  $100 \text{ km s}^{-1}$  for all of the galaxies. In Paper I a correction for  $1+z$  stretching of the spectra was applied to the velocity dispersions. Since the spectra are binned in equal steps in  $\log v$  before the velocity dispersion is determined, the correction for  $1+z$  stretching is inherent in the method and the correction in Paper I should not have been applied. The values of  $\sigma$  listed in Table 1 for those galaxies reported in Paper I have had this erroneous (but small) correction removed.

## c) Comparison with Other Authors

We compare our velocity dispersion measurements with those of seven other authors (Whitmore and Kirshner 1981, hereafter WK; Schechter 1980, hereafter S80; Sargent *et al.* 1977, hereafter SSBS; Faber and Jackson 1976, hereafter FJ; Tonry 1980, hereafter T80; Davies 1981, hereafter D81; and Faber, Burstein, and Dressler 1977, hereafter FBD) in Table 2. Only four BCM galaxies in Abell clusters have been measured by these authors. The brightest member of A401 has a measured velocity dispersion of  $480 \pm 120 \text{ km s}^{-1}$  by FBD from the sodium D line. However, they estimate that the rest of the spectrum indicates a value of  $350 \text{ km s}^{-1}$ . This estimate is in good agreement with the velocity dispersion of  $367 \text{ km s}^{-1}$  measured here. The velocity dispersion in NGC 6166 (the BCM galaxy in A2199) determined here is much larger than the  $350 \text{ km s}^{-1}$  determined by FJ; however, it was one of our poorest determinations and the drift was unusually large ( $D \approx 130 \text{ km s}^{-1}$ ). We have therefore adopted a weighted mean of our measurement and that of FJ, with double weight given to the FJ value. The adopted velocity dispersion of NGC 6166 is  $380 \text{ km s}^{-1}$ .

There is considerable overlap with these authors in the sample of elliptical galaxies observed here. In general our dispersions agree quite well with WK and S80 and are approximately 6% larger than the others. Since the internal errors are typically about 10%, the overall agreement with these other authors is satisfactory.

## III. SURFACE PHOTOMETRY

## a) The Sample

Direct CCD images were obtained for a sample of 19 BCM galaxies in Abell clusters and eight BCM galaxies in MKW or

AWM poor clusters. The surface photometry standard NGC 3379 (de Vaucouleurs and Capaccioli 1979) was also observed. Of the BCM galaxies in Abell clusters, three have previously published surface brightness profiles to faint limits (O76). In addition, Thuan and Romanishin (1981, hereafter TR) have published profiles for five of the poor cluster BCM galaxies in this sample. We have determined velocity dispersions for 16 of the 19 Abell cluster BCM galaxies, and all eight of the poor cluster BCMs. The velocity dispersion of a 17th Abell cluster BCM (in A2029) is published by Dressler (1979). Including the photometry of O76 and TR gives us a sample of 31 BCM galaxies with both surface photometry and velocity dispersions. We list all of the galaxies observed for surface photometry in Table 3 along with the number of exposures, the exposure times and the telescope used.

## b) Observations and Analysis

CCD cameras were used on the McGraw-Hill Observatory 1.3 m telescope and the Kitt Peak National Observatory No. 1 0.9 m telescope to obtain images of the 28 galaxies listed in Table 3. The CCD camera used on the McGraw-Hill Observatory telescope was developed by Dr. Donald York and Princeton University. These data were obtained in three runs, 1981 December and 1982 May at McGraw-Hill Observatory and 1982 June at KPNO. Most of the galaxies were observed with moonless skies. Although some of the nights were partly cloudy, most of them were photometric. Surface photometry in partly cloudy weather is reasonable as long as the exposure time is long compared with the time it takes for a cloud to cross the field, since the entire field will be obscured in the same way. However, the absolute calibration will not be good under such conditions. By good fortune, the last night of each run was

TABLE 2  
COMPARISON WITH OTHER AUTHORS<sup>a</sup>

Galaxy	$\sigma$	WK	S80	SSBS	FJ	T80	D81	FBD
A401 .....	$367 \pm 35$	...	...	...	...	...	...	$\left\{ \begin{array}{l} 480 \pm 120 \\ 350^b \end{array} \right.$
A779 .....	$372 \pm 26$	...	...	...	...	$301 \pm 11$	...	...
NGC 533 .....	$284 \pm 35$	...	...	...	...	$301 \pm 14$	...	...
NGC 636 .....	$174 \pm 17$	...	$176 \pm 14$	...	...	...	...	...
NGC 741 .....	$345 \pm 28$	...	...	$318 \pm 35$	...	$268 \pm 22$	...	...
NGC 1052 .....	$192 \pm 33$	...	$212 \pm 19$	$187 \pm 16$	...	...	...	...
NGC 1400 .....	$250 \pm 29$	...	$273 \pm 25$	...	...	$270 \pm 16$	...	...
NGC 1426 .....	$153 \pm 22$	...	...	$151 \pm 8$	...	$177 \pm 22$	...	...
NGC 1600 .....	$363 \pm 28$	...	...	...	...	$352 \pm 23$	...	...
NGC 1700 .....	$267 \pm 20$	...	...	...	...	$241 \pm 14$	...	...
NGC 2768 .....	$207 \pm 23$	...	...	...	...	$218 \pm 23$	...	...
NGC 3158 .....	$390 \pm 30$	...	...	...	...	$372 \pm 20$	...	...
NGC 4374 .....	$299 \pm 21^c$	$282 \pm 30$	$298 \pm 18$	...	$285 \pm 15$	$319 \pm 9$	$280 \pm 14$	...
NGC 4406 .....	$244 \pm 19$	$283 \pm 18$	$231 \pm 12$	...	$265 \pm 19$	$267 \pm 7$	$257 \pm 12$	...
NGC 4467 .....	$102 \pm 17$	...	...	...	$\leq 150$	...	...	...
NGC 4472 .....	$352 \pm 25^c$	$300 \pm 23$	...	...	$295 \pm 6$	$316 \pm 8$	$308 \pm 20$	...
NGC 4473 .....	$203 \pm 12$	...	...	...	...	$228 \pm 7$	...	...
NGC 4486 .....	$343 \pm 40^c$	$358 \pm 29$	$330 \pm 37$	...	$315 \pm 28$	$348 \pm 12$	...	...
NGC 4564 .....	$245 \pm 20$	...	...	...	...	$285 \pm 17$	...	...
NGC 4649 .....	$324 \pm 25$	...	$383 \pm 33$	...	$360 \pm 36$	$341 \pm 13$	...	...
NGC 4889 .....	$428 \pm 31$	...	...	...	$400 \pm 40$	$411 \pm 20$	...	...
NGC 6166 .....	$439 \pm 46$	...	...	...	$350 \pm 35$	...	...	...
NGC 7619 .....	$336 \pm 23^c$	...	...	...	...	$285 \pm 20$	...	...
NGC 7626 .....	$292 \pm 25^c$	...	$267 \pm 38$	$263 \pm 17$	...	$222 \pm 23$	...	...
Average factors .....		1.01	0.99	1.06	1.07	1.06	1.05	...

<sup>a</sup> Other authors: WK = Whitmore and Kirshner 1981; S80 = Schechter 1980; SSBS = Sargent *et al.* 1977; FJ = Faber and Jackson 1976; T80 = Tonry 1980; D81 = Davies 1981; FBD = Faber, Burstein, and Dressler 1977.

<sup>b</sup> Value excluding the the sodium D line.

<sup>c</sup> Averages of the values in Table 1.

TABLE 3  
SURFACE PHOTOMETRY OBSERVATIONS

Galaxy	Cluster	Number of Exposures	Exposure Time (minutes)	Telescope
...	A150	2	15 30	MGH 1.3 m
...	A401	2	30 30	MGH 1.3 m
...	A496	3	30 30 30	MGH 1.3 m
...	A505	2	15 30	MGH 1.3 m
...	A994	2	15 60	MGH 1.3 m
...	A1177	2	15 50	MGH 1.3 m
...	A1631	2	5 60	KPNO No. 1 0.9 m
...	A1904	2	2 60	KPNO No. 1 0.9 m
...	A2029	2	5 60	KPNO No. 1 0.9 m
...	A2052	1	30	MGH 1.3 m
...	A2107	2	5 60	KPNO No. 1 0.9 m
...	A2124	2	5 60	KPNO No. 1 0.9 m
...	A2147	1	5	KPNO No. 1 0.9 m
NGC 6086	A2162	2	5 60	KPNO No. 1 0.9 m
...	A2366	2	5 60	KPNO No. 1 0.9 m
...	A2457	2	5 40	KPNO No. 1 0.9 m
...	A2589	4	{ 5 30 30 30	{ KPNO No. 1 0.9 m MGH 1.3 m
NGC 7768	A2666	3	5 30 30	MGH 1.3 m
...	A2670	1	30	MGH 1.3 m
NGC 5400	MKW 5	2	10 60	MGH 1.3 m
NGC 2804	AWM 1	2	30 30	MGH 1.3 m
NGC 4213	AWM 2	2	5 60	KPNO No. 1 0.9 m
NGC 5629	AWM 3	1	5	KPNO No. 1 0.9 m
...	AWM 4	1	5	KPNO No. 1 0.9 m
NGC 6269	AWM 5	2	5 60	KPNO No. 1 0.9 m
IC 4062	AWM 6	1	60	MGH 1.3 m
NGC 1129	AWM 7	3	5 15 30	MGH 1.3 m
NGC 3379	M96 group	2	2 30	MGH 1.3 m

photometric, so we obtained a short exposure of each of the galaxies which had been observed under nonphotometric conditions. These short exposures were used for the absolute calibration for those galaxies.

RCA CCD chips were used in both cameras. The 1981 December data were digitized at 13.0 electrons per analog to digital convertor unit (ADU), the 1982 May data at 40.0 electrons per ADU, and the KPNO (1982 June) data at 14.8 electrons per ADU. The choices of digitization were made to get the maximum signal in the low surface brightness regions in a long exposure. This resulted in the saturation of the analog to digital conversion near the centers of some of the galaxies. A short exposure was used to determine the luminosity distribution near the center in those cases. Both telescopes were used at  $f/7.5$ , which gave a field of  $5'.6 \times 3'.5$  for the McGraw-Hill observations and  $7'.3 \times 4'.6$  for the KPNO observations in the  $512 \times 320$  pixels. The scale was  $0.65$  arcsec pixel $^{-1}$  for the McGraw-Hill observations and  $0.85$  arcsec pixel $^{-1}$  for the KPNO observations. The readout noise was about 75 electrons for each camera.

Along with the images of the galaxy, dark frames and sky flat frames were obtained at both telescopes. Dome flat frames and bias frames were also obtained at KPNO. Standard stars with galaxy-like colors were obtained each night of each run for absolute calibration. These were typically in Kitt Peak videocamera/CCD standard fields. All images were obtained with a  $V$ -like filter. The filter used in the 1981 December run has a peak transmission at about  $5300 \text{ \AA}$  and essentially no transmission short of  $4850 \text{ \AA}$  or longward of  $6000 \text{ \AA}$ . The filter used in the other runs was the KPNO No. 18  $V$ -filter, which has a peak transmission at about  $5400 \text{ \AA}$  and drops essentially to zero at  $4750$  and  $7000 \text{ \AA}$ .

The McGraw-Hill data were bias-subtracted using an over-read area of 20 rows, and dark-subtracted using an average of all of the dark frames obtained during the run. The data frame was then flattened by dividing it by an average sky flat which had been cleaned of stars and galaxies. The KPNO data were bias-subtracted using the bias frames obtained on the night of the observation. Each frame was then flattened by dividing by an average of the dome flats taken on the same night. Interference fringes caused by the  $5577 \text{ \AA}$  night-sky line were present in the KPNO data. This was dealt with by forming a composite sky frame: the average of all the sky frames cleaned of stars. This composite sky was multiplied by a constant and then subtracted from the data frame. The resulting frame was displayed on the KPNO interactive picture processing system (IPPS) Comtal display unit with very high contrast. A second guess of the constant needed to multiply the sky frame by was made by looking at the residual fringes. This was necessary because the night-sky line varies in strength relative to the continuum. This process was continued until the residual fringes could no longer be seen on the display unit. At that time the residual fringe amplitude was smaller than 1% of the sky.

A plane was fitted to the sky background for those galaxies which had no bright objects near the corners of the frame, so that we could measure the sky in all four corners. This plane was subtracted from the data frame and the average value added back. This removes any large-scale gradient in the sky across the frame. The gradient measured in this way was typically 1%–2% of the sky.

Once the frames were flattened, the fringes removed, and the gradient in the sky removed, bad columns, rows, and pixels were replaced with zeros. Stars and galaxies in the field were removed by replacing with zeros all of the pixels within circles

of approximately twice the radius of the contour where they were about 1% of the sky. This cleaning of stars and galaxies and of the bad pixels, rows, and columns left about 60%–70% of the frame with data.

Ellipses were then fitted to the remaining data (zeros were ignored) at 1 pixel intervals in the semimajor axis, using the method of Kent (1983) as adapted by Hegyi, Gudehus, and Sharkin (1983). This method is similar to that of Young *et al.* (1979). The center of the ellipse, the position angle, and the ellipticity were obtained for each isophote down to a surface brightness of approximately  $25 \text{ mag arcsec}^{-2}$ . The center of the ellipse, the position angle, and the ellipticity were then smoothed with radius. In all but one case the center was fixed as the average of the centers of all of the isophotes. For A2666 the center position clearly varied as a function of the semimajor axis and was smoothed by fitting a straight line to the unsmoothed values of the center position. The center of the isophotes in this galaxy changes by about  $5''$  from the center to the edge of the galaxy. This variation appears to be real and may be a clue to the true shape of this galaxy. The values of the position angle and ellipticity determined from the individual fits to each isophote had a large amount of scatter. These quantities were smoothed using one or more polynomials over different ranges in radii. The order of the polynomial was chosen to best represent the trend in the unsmoothed data. A second-order polynomial was used in many cases, and in a few cases the data were best described by a higher (up to 5th) order polynomial. This process continued until a smooth curve was obtained which was a good representation of the unsmoothed data.

The values of each pixel along the ellipses defined by the smoothed quantities were averaged at intervals of 1 pixel in the semimajor axis. These averages are the surface brightnesses of the isophotes. Beyond that, the profile was extended as far as the data would allow by assuming contours of the same center, ellipticity, and position angles as the last smoothed one. The sky level was determined from the average of the pixel values in areas near the corners of the frame, and then subtracted. Isophotes were averaged in roughly logarithmic bins and changed into  $\text{mag arcsec}^{-2}$  using the calibration stars observed the same night as the galaxy. The atmospheric extinction was  $0.20 \text{ mag per air mass}$ .

In this way a table of surface brightness,  $\mu_v$  (in  $\text{mag arcsec}^{-2}$ ), versus the log of the geometric mean of the semimajor and semiminor axes [ $\log r \equiv \log(ab)^{1/2}$ ] was produced. As mentioned before, the inner parts of many of the long exposures were saturated, so in most cases a short exposure was also obtained. In those cases a composite profile was produced using the short exposure exclusively near the center, the long exposure exclusively far from the center, and an average of the two exposures in between. In some cases more than one long exposure was obtained, and the results have been averaged together at all radii. The long exposures of A2147, AWM 3, and AWM 4 were lost as a result of a problem with the autoguider on the Kitt Peak No. 1 0.9 m telescope. In those cases only a short exposure was obtained.

The final composite surface brightness profiles of the BCM galaxies corrected for galactic absorption using the model of Sandage (1973) and  $K$ -corrected using the tables of Pence (1976) are listed in Table 4. These  $K$ -corrections include only the  $1+z$  stretching of the spectrum and the spectral energy distribution of the galaxy. The BCM galaxies were assumed to have spectral energy distributions like those of E galaxies.

Where the surface brightness is given in units of  $\text{mag arcsec}^{-1}$ , no correction for  $(1+z)^4$  dimming has been made. However, when the surface brightnesses of the galaxies are compared with each other, units of  $L_\odot \text{ pc}^{-2}$  are used, assuming  $H_0 = 50 \text{ km s}^{-1} \text{ Mpc}^{-1}$  and  $q_0 = 0$ . These units correct the surface brightness to the local rest frame of the galaxy.

The position angle and ellipticities are also listed in Table 4. The average axial ratio,  $b/a$ , is  $0.7 \pm 0.03$  at a surface brightness of  $24 \text{ mag arcsec}^{-2}$  for these galaxies. Leir and van den Bergh (1977) found a similar value for the Bautz-Morgan type I clusters in their sample. However, when they excluded the more distant clusters, they found a smaller value (flatter galaxies). The BCM galaxies in Bautz-Morgan types II–III and III clusters in Leir and van den Bergh's (1977) sample were not as flat ( $\langle b/a \rangle = 0.83$  for all of the Bautz-Morgan type III BCM galaxies). Most of the galaxies in this sample become more elliptical with radius. Since a nearby galaxy covers more area on a photographic plate than a distant galaxy, it is easier to see down to a faint isophote on a nearby galaxy. This may explain why Leir and van den Bergh (1977) found the nearer BCM galaxies to be flatter on average than their entire sample.

### c) Comparison with Other Authors

During each run, one or more galaxies with a previously published surface brightness profile by O76 or TR were observed. In addition, the surface photometry standard galaxy NGC 3379 (de Vaucouleurs and Capaccioli 1979) was observed in the 1981 December run at McGraw-Hill Observatory. Our profile of NGC 3379 is compared with that of de Vaucouleurs and Capaccioli (1979) in Figure 1. The zero-point shift was arbitrary and represents a  $B-V$  of  $0.85 \text{ mag}$ . NGC 3379 is a nearby galaxy and is larger than the  $5.6 \times 3.5$  field of the CCD. The surface brightness is  $22.7 \text{ mag arcsec}^{-2}$  at a radius of  $100''$ , the radius of the edge of the frame in the short dimension. We chose a sky value so that the last point in Figure 1 was in fair agreement with the standard profile. The last point is not at zero difference in Figure 1, since the average shift was determined after the sky value was set. Our profile is fainter than the standard profile in the central  $1''0$  because of seeing, but after that the agreement is better than  $0.08 \text{ mag}$  throughout. This, of course, does not tell us how accurate the absolute photometry or the sky determinations are, but the comparison of this galaxy does suggest that the relative pho-

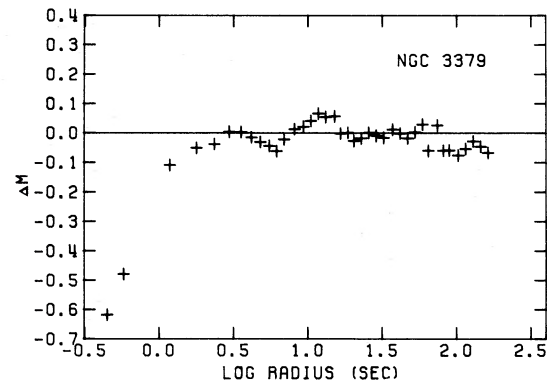


FIG. 1.—Comparison of our photometry of NGC 3379 with that of de Vaucouleurs and Capaccioli (1979).  $\Delta\mu$  is the de Vaucouleurs and Capaccioli profile minus ours. The zero-point shift was arbitrary and represents a  $B-V$  of  $0.85 \text{ mag}$ . At radii less than  $1''$  the difference is large because of seeing effects. The agreement is better than  $0.08 \text{ mag}$  peak to peak beyond that.

TABLE 4  
SURFACE PHOTOMETRY PROFILES

A150				A401				A496				A505			
FWHM of PSF 2.3				FWHM of PSF 2.0				FWHM of PSF 3.0				FWHM of PSF 4.0			
Log r (arcsec)	$\mu_V$	PA	E	Log r (arcsec)	$\mu_V$	PA	E	Log r (arcsec)	$\mu_V$	PA	E	Log r (arcsec)	$\mu_V$	PA	E
-0.32	19.68	135	0.12	-0.37	19.99	92	0.00	-0.35	19.28	16	0.18	-0.36	19.40	105	0.00
-0.06	19.79	135	0.12	-0.22	20.08	92	0.00	-0.20	19.34	16	0.18	-0.21	19.46	131	0.14
0.11	19.96	132	0.08	0.07	20.29	80	0.14	0.07	19.45	117	0.04	0.10	19.55	131	0.13
0.23	20.15	133	0.08	0.25	20.59	73	0.18	0.26	19.62	147	0.05	0.27	19.66	132	0.13
0.48	20.55	134	0.08	0.37	20.87	72	0.16	0.39	19.82	140	0.03	0.40	19.82	132	0.12
0.56	20.75	4	0.08	0.46	21.08	62	0.17	0.49	20.02	144	0.07	0.49	20.00	133	0.11
C 63	20.99	179	0.08	0.53	21.26	55	0.18	0.56	20.19	158	0.08	0.57	20.18	133	0.11
0.68	21.19	4	0.07	0.59	21.41	46	0.19	0.63	20.35	158	0.08	0.63	20.36	134	0.10
0.73	21.40	1	0.08	0.65	21.57	45	0.20	0.68	20.50	157	0.10	0.69	20.54	134	0.10
0.78	21.58	172	0.08	0.70	21.70	43	0.21	0.73	20.63	161	0.12	0.74	20.71	134	0.09
0.84	21.80	16E	0.09	0.74	21.85	37	0.22	0.77	20.75	171	0.12	0.78	20.87	135	0.09
0.89	22.04	163	0.12	0.80	22.02	36	0.23	0.83	20.90	173	0.13	0.84	21.09	135	0.08
0.96	22.28	167	0.16	0.86	22.22	36	0.24	0.89	21.09	170	0.16	0.91	21.35	136	0.07
1.01	22.47	169	0.14	0.91	22.36	34	0.27	0.95	21.26	173	0.16	0.98	21.58	137	0.07
1.05	22.62	171	0.16	C.95	22.51	32	0.32	1.00	21.40	172	0.19	1.03	21.77	138	0.06
1.10	22.81	175	0.16	1.00	22.62	34	0.35	1.05	21.56	176	0.16	1.08	21.97	139	0.05
1.15	22.98	175	0.18	1.04	22.77	35	0.40	1.09	21.72	179	0.21	1.14	22.19	140	0.05
1.20	23.16	175	0.21	1.10	22.93	35	0.40	1.15	21.89	175	0.23	1.19	22.40	141	0.04
1.24	23.32	175	0.21	1.15	23.09	35	0.40	1.20	22.05	176	0.21	1.24	22.61	142	0.04
1.28	23.50	175	0.19	1.19	23.24	35	0.40	1.24	22.20	174	0.18	1.29	22.79	144	0.03
1.32	23.65	175	0.23	1.24	23.40	35	0.40	1.28	22.31	176	0.24	1.33	22.98	145	0.02
1.36	23.83	175	0.25	1.28	23.58	35	0.40	1.33	22.47	176	0.28	1.38	23.22	147	0.02
1.41	24.05	175	0.26	1.33	23.76	35	0.40	1.36	22.62	176	0.28	1.43	23.48	148	0.02
1.46	24.23	175	0.24	1.39	24.01	35	0.40	1.42	22.79	176	0.28	1.48	23.76	151	0.01
1.51	24.46	176	0.24	1.44	24.37	35	0.40	1.47	23.01	176	0.28	1.53	24.07	153	0.01
1.56	24.67	176	0.24	1.50	24.62	35	0.40	1.53	23.22	176	0.28	1.59	24.30	157	0.01
1.60	24.85	176	0.24	1.55	24.93	35	0.40	1.58	23.48	176	0.28	1.64	24.51	160	0.01
1.65	25.08	176	0.24	1.60	24.98	35	0.40	1.63	23.66	176	0.29	1.69	24.80	163	0.01
1.70	25.31	176	0.24	1.64	25.10	35	0.40	1.67	23.85	175	0.32	1.73	25.04	167	0.01
1.76	25.45	176	0.24	1.69	25.29	35	0.40	1.72	24.04	175	0.32	1.78	25.33	171	0.01
1.81	25.75	176	0.24	1.74	25.49	35	0.40	1.77	24.23	175	0.32	1.83	25.51	172	0.02
1.85	25.95	176	0.24	1.79	25.88	35	0.40	1.82	24.41	175	0.32	1.88	25.78	172	0.02
1.90	26.32	176	0.24	1.84	26.01	35	0.40	1.87	24.62	175	0.32	1.93	25.98	172	0.02
1.95	26.48	176	0.24	1.89	26.46	35	0.40	1.92	24.90	175	0.32	1.99	25.76	172	0.02
2.01	26.53	176	0.24					1.97	25.21	175	0.32	2.04	26.24	172	0.02
2.06	26.73	176	0.24					2.02	25.59	175	0.32	2.09	26.41	172	0.02
2.10	26.64	176	0.24					2.07	25.95	175	0.32	2.14	27.28	172	0.02
2.15	26.49	176	0.24					2.12	26.20	175	0.32	2.19	27.79	172	0.02
2.20	27.52	176	0.24					2.17	26.46	175	0.32				
2.24	26.04	176	0.24					2.22	26.77	175	0.32				

A994				A1177				A1631				A1904			
FWHM of PSF 2.2				FWHM of PSF 2.8				FWHM of PSF 2.5				FWHM of PSF 2.4			
Log r (arcsec)	$\mu_V$	PA	E	Log r (arcsec)	$\mu_V$	PA	E	Log r (arcsec)	$\mu_V$	PA	E	Log r (arcsec)	$\mu_V$	PA	E
-0.33	16.33	133	0.01	-0.34	18.20	55	0.11	-0.23	18.21	69	0.23	-0.24	19.09	4	0.20
-0.18	18.46	133	0.01	-0.19	18.41	55	0.11	-0.06	18.27	69	0.22	-0.13	19.16	4	0.20
0.09	18.69	133	0.01	0.10	18.63	55	0.11	0.22	18.49	61	0.23	0.17	19.45	7	0.18
0.26	19.01	133	0.09	0.26	18.91	55	0.11	0.39	18.79	64	0.23	0.36	19.86	11	0.22
0.38	19.33	139	0.15	0.38	19.21	55	0.11	0.51	19.06	64	0.23	0.48	20.25	15	0.23
0.47	19.62	148	0.19	0.49	19.52	55	0.11	0.59	19.28	53	0.23	0.57	20.62	18	0.23
0.54	19.89	150	0.22	0.56	19.80	55	0.10	0.67	19.51	53	0.23	0.65	20.97	22	0.23
0.60	20.12	152	0.25	0.63	20.08	55	0.10	0.73	19.71	53	0.23	0.72	21.23	28	0.23
0.65	20.34	154	0.27	0.69	20.29	55	0.10	0.78	19.87	53	0.23	0.78	21.44	28	0.23
0.70	20.52	154	0.29	0.74	20.48	55	0.10	0.83	20.02	53	0.23	0.83	21.64	31	0.23
0.73	20.69	150	0.31	0.78	20.63	55	0.10	0.88	20.16	53	0.23	0.88	21.80	26	0.24
0.79	20.91	150	0.34	0.84	20.85	55	0.10	0.93	20.35	53	0.23	0.94	22.03	29	0.24
0.85	21.16	150	0.37	0.91	21.08	55	0.10	1.01	20.56	52	0.23	1.00	22.30	42	0.24
0.91	21.46	151	0.35	0.97	21.28	55	0.10	1.06	20.77	52	0.23	1.06	22.53	42	0.25
0.97	21.70	151	0.35	1.03	21.45	55	0.10	1.11	20.98	52	0.23	1.12	22.73	42	0.25
1.01	21.91	152	0.35	1.07	21.59	55	0.10	1.16	21.17	51	0.24	1.16	22.97	42	0.25
1.07	22.17	152	0.35	1.13	21.76	55	0.10	1.22	21.39	51	0.24	1.21	23.19	42	0.26
1.12	22.44	152	0.35	1.18	21.92	55	0.09	1.27	21.63	51	0.24	1.27	23.44	42	0.26
1.17	22.69	153	0.35	1.23	22.09	55	0.09	1.32	21.85	50	0.24	1.31	23.67	42	0.27
1.21	22.93	154	0.35	1.27	22.25	55	0.09	1.37	22.06	50	0.24	1.36	23.84	42	0.27
1.26	23.17	154	0.35	1.32	22.39	55	0.09	1.42	22.27	49	0.24	1.40	23.98	42	0.28
1.31	23.44	155	0.35	1.36	22.53	55	0.09	1.47	22.48	49	0.25	1.45	24.19	42	0.29
1.36	23.71	156	0.35	1.41	22.67	55	0.10	1.52	22.69	48	0.25	1.49	24.41	42	0.29
1.41	24.08	157	0.35	1.46	22.87	55	0.10	1.56	22.90	48	0.25	1.54	24.58	42	0.30
1.46	24.35	158	0.35	1.51	23.16	55	0.10	1.61	23.18	47	0.26	1.59	24.86	42	0.31
1.52	24.57	159	0.35	1.57	23.40	55	0.11	1.66	23.44	46	0.26	1.65	25.07	42	0.32
1.57	24.87	160	0.35	1.62	23.63	55	0.12	1.72	23.76	45	0.27	1.69	25.32	42	0.33
1.62	25.41	162	0.35	1.66	23.80	55	0.13	1.76	24.09	44	0.27	1.74	25.84	42	0.34
1.67	25.91	163	0.35	1.71	23.98	55	0.15	1.81	24.35	42	0.28	1.79	26.08	42	0.35
1.72	26.30	165	0.35	1.76	24.16	55	0.17	1.85	24.69	41	0.29	1.83	26.38	42	0.36
1.77	26.72	167	0.35	1.80	24.31	55	0.21	1.90	24.98	39	0.30				
1.82	27.58	170	0.35	1.83	24.47	55	0.28	1.95	25.29	38	0.31				
1.87	27.98	172	0.35	1.85	24.59	55	0.38	1.99	25.43	36	0.32				
1.92	28.60	174	0.35	1.87	24.67	55	0.49	2.04	25.57	34	0.32				
				1.91	25.01	55	0.50	2.09	25.91	34	0.32				
				1.96	25.28	55	0.50	2.14	26.33	34	0.32				
				2.01	25.63	55	0.50	2.19	27.10	34	0.32				
				2.06	26.14	55	0.50	2.24	27.59	34	0.32				
				2.11	27.00	55	0.50	2.29	28.49	34	0.32				

TABLE 4—Continued

A2029				A2052				A2107				A2124			
FWHM of PSF 2.4				FWHM of PSF 2.0				FWHM of PSF 4.0				FWHM of PSF 2.6			
Log r	$\mu_V$	PA	E	Log r	$\mu_V$	PA	E	Log r	$\mu_V$	PA	E	Log r	$\mu_V$	PA	E
(arcsec)				(arcsec)				(arcsec)				(arcsec)			
-0.22	19.67	22	0.03	-0.33	19.20	164	0.00	-0.23	19.28	89	0.06	-0.25	19.42	3	0.06
-0.08	19.74	19	0.09	-0.18	19.31	164	0.00	-0.10	19.34	89	0.06	-0.09	19.57	3	0.06
0.21	19.90	19	0.11	0.10	19.48	77	0.06	0.20	19.52	89	0.06	0.21	19.91	179	0.07
0.38	20.09	19	0.14	0.28	19.72	50	0.08	0.37	19.73	89	0.06	0.39	20.29	175	0.08
0.47	20.28	19	0.16	0.41	19.98	44	0.05	0.50	19.96	89	0.06	0.51	20.63	172	0.09
0.57	20.50	19	0.18	0.51	20.18	39	0.03	0.59	20.17	87	0.06	0.61	20.92	169	0.10
0.64	20.71	20	0.21	0.58	20.33	37	0.06	0.69	20.46	135	0.01	0.69	21.17	166	0.10
0.71	20.90	20	0.23	0.64	20.45	37	0.11	0.75	20.62	100	0.08	0.75	21.35	163	0.11
0.76	21.07	20	0.25	0.69	20.57	36	0.14	0.80	20.78	107	0.12	0.81	21.50	160	0.12
0.81	21.22	20	0.27	0.73	20.66	34	0.18	0.86	20.96	110	0.13	0.86	21.67	158	0.13
0.86	21.36	20	0.30	0.77	20.76	28	0.17	0.89	21.08	109	0.13	0.90	21.81	156	0.13
0.91	21.54	20	0.32	0.83	20.88	28	0.20	0.95	21.32	112	0.13	0.96	22.00	153	0.14
0.97	21.77	21	0.36	0.89	21.03	28	0.21	1.02	21.56	111	0.14	1.03	22.22	150	0.16
1.03	21.96	21	0.39	0.95	21.15	28	0.24	1.09	21.78	113	0.15	1.09	22.44	147	0.17
1.08	22.12	21	0.41	0.99	21.27	28	0.26	1.14	21.97	111	0.17	1.16	22.65	144	0.19
1.12	22.29	21	0.43	1.04	21.39	28	0.27	1.18	22.16	112	0.17	1.20	22.78	143	0.20
1.17	22.46	22	0.44	1.09	21.53	28	0.28	1.23	22.35	113	0.18	1.25	23.01	141	0.21
1.22	22.63	22	0.45	1.14	21.70	28	0.28	1.29	22.56	114	0.17	1.31	23.23	140	0.22
1.27	22.83	22	0.46	1.19	21.86	28	0.28	1.34	22.80	116	0.17	1.36	23.33	139	0.23
1.31	23.01	23	0.46	1.24	22.01	28	0.28	1.39	22.99	115	0.17	1.40	23.60	138	0.24
1.34	23.07	23	0.46	1.28	22.17	28	0.28	1.44	23.21	113	0.15	1.45	23.95	138	0.25
1.39	23.27	23	0.46	1.33	22.34	28	0.28	1.48	23.44	111	0.18	1.50	24.18	139	0.26
1.43	23.42	24	0.46	1.38	22.51	28	0.28	1.49	23.43	112	0.30	1.55	24.57	139	0.26
1.48	23.60	24	0.47	1.43	22.73	28	0.28	1.55	23.68	114	0.28	1.61	24.96	140	0.27
1.53	23.88	25	0.48	1.48	22.95	28	0.28	1.59	23.89	118	0.31	1.66	25.47	140	0.27
1.58	24.12	25	0.50	1.54	23.19	28	0.28	1.64	24.08	120	0.35	1.71	25.79	140	0.28
1.63	24.34	25	0.51	1.59	23.40	28	0.28	1.71	24.55	121	0.29	1.76	26.34	140	0.29
1.67	24.51	25	0.52	1.64	23.60	28	0.28	1.77	24.83	136	0.26	1.79	26.55	138	0.30
1.72	24.70	25	0.51	1.69	23.81	28	0.28	1.81	25.07	114	0.28	1.83	27.36	136	0.32
1.77	24.92	25	0.51	1.74	24.02	28	0.28	1.84	25.30	114	0.32	1.88	27.80	136	0.36
1.82	25.35	24	0.52	1.79	24.26	28	0.28	1.90	25.66	115	0.31	1.93	28.52	136	0.37
1.86	25.78	23	0.55	1.84	24.52	28	0.28	1.97	26.09	101	0.22				
1.94	26.11	22	0.48	1.89	24.76	28	0.28	2.01	26.37	103	0.25				
1.99	26.29	22	0.48	1.94	24.98	28	0.28	2.04	26.59	99	0.32				
2.04	26.53	22	0.48	1.99	25.35	28	0.28	2.09	26.90	99	0.32				
2.09	26.84	22	0.48	2.04	25.76	28	0.28	2.14	27.09	99	0.32				
2.14	27.36	22	0.48	2.09	26.28	28	0.28	2.19	27.75	99	0.32				
2.19	27.54	22	0.48	2.14	26.71	28	0.28	2.24	28.72	99	0.32				
2.24	28.04	22	0.48	2.19	27.05	28	0.28								
2.29	28.15	22	0.48												

A2147				A2162				A2366				A2457			
FWHM of PSF 2.7				FWHM of PSF 2.4				FWHM of PSF 2.0				FWHM of PSF 2.7			
Log r	$\mu_V$	PA	E	Log r	$\mu_V$	PA	E	Log r	$\mu_V$	PA	E	Log r	$\mu_V$	PA	E
(arcsec)				(arcsec)				(arcsec)				(arcsec)			
-0.26	19.08	17	0.19	-0.26	18.07	31	0.14	-0.23	18.60	154	0.00	-0.25	19.21	140	0.14
-0.11	19.15	17	0.19	-0.11	18.18	15	0.18	-0.07	18.75	154	0.00	-0.11	19.23	80	0.17
0.19	19.35	17	0.19	0.19	18.47	14	0.18	0.22	19.18	160	0.05	0.19	19.54	80	0.17
0.36	19.61	17	0.20	0.37	18.84	13	0.19	0.39	19.73	156	0.06	0.37	19.95	80	0.17
0.49	19.86	17	0.20	0.49	19.25	12	0.20	0.52	20.22	147	0.09	0.49	20.35	80	0.17
0.58	20.12	17	0.21	0.58	19.61	11	0.20	0.61	20.62	143	0.08	0.58	20.72	81	0.17
0.66	20.35	17	0.21	0.66	19.94	10	0.21	0.69	20.97	143	0.09	0.66	20.97	81	0.17
0.73	20.56	17	0.21	0.73	20.23	9	0.22	0.76	21.26	143	0.09	0.73	21.25	81	0.17
0.78	20.75	17	0.22	0.78	20.48	8	0.23	0.82	21.51	143	0.09	0.79	21.47	81	0.18
0.83	20.93	16	0.22	0.83	20.68	7	0.23	0.87	21.74	143	0.09	0.84	21.68	81	0.18
0.88	21.09	16	0.23	0.88	20.86	7	0.24	0.91	21.93	143	0.09	0.88	21.84	81	0.18
0.94	21.29	16	0.24	0.93	21.09	6	0.25	0.97	22.20	143	0.09	0.94	22.09	81	0.18
1.00	21.54	16	0.25	1.01	21.36	4	0.26	1.04	22.49	143	0.09	1.01	22.39	82	0.18
1.06	21.76	16	0.25	1.06	21.55	3	0.27	1.10	22.74	143	0.09	1.08	22.73	82	0.19
1.11	21.92	15	0.26	1.10	21.77	2	0.28	1.15	22.92	143	0.10	1.13	23.01	82	0.19
1.16	22.10	15	0.27	1.15	21.97	1	0.29	1.20	23.10	143	0.10	1.18	23.20	82	0.19
1.20	22.28	15	0.29	1.20	22.18	0	0.30	1.25	23.28	143	0.10	1.23	23.46	83	0.20
1.26	22.51	14	0.30	1.25	22.42	0	0.31	1.31	23.47	143	0.10	1.28	23.75	83	0.20
1.30	22.68	14	0.31	1.30	22.67	179	0.30	1.36	23.66	143	0.11	1.33	23.96	83	0.21
1.34	22.88	14	0.33	1.35	22.84	179	0.31	1.40	23.87	143	0.11	1.37	24.18	84	0.21
1.38	23.06	13	0.35	1.39	23.01	179	0.32	1.45	24.09	143	0.11	1.42	24.39	84	0.22
1.42	23.25	13	0.37	1.43	23.14	179	0.32	1.49	24.26	143	0.12	1.46	24.66	85	0.23
1.46	23.45	12	0.39	1.48	23.30	179	0.33	1.54	24.57	143	0.12	1.51	24.86	85	0.24
1.50	23.56	11	0.42	1.53	23.52	179	0.35	1.59	24.92	143	0.13	1.56	25.15	86	0.25
1.54	23.55	11	0.45	1.58	23.71	178	0.36	1.64	25.19	143	0.13	1.61	25.40	87	0.26
1.58	23.83	10	0.49	1.63	23.90	178	0.38	1.70	25.35	143	0.14	1.66	25.86	88	0.27
1.62	23.83	9	0.53	1.67	24.09	178	0.40	1.75	25.62	143	0.15	1.71	26.17	88	0.29
1.65	23.97	8	0.57	1.71	24.25	177	0.42	1.79	25.83	143	0.16	1.75	26.14	90	0.31
1.67	23.96	7	0.61	1.75	24.42	177	0.44	1.84	26.24	143	0.17	1.79	26.52	91	0.33
1.70	23.98	6	0.65	1.79	24.64	176	0.47	1.88	26.27	143	0.18	1.83	26.75	92	0.36
1.73	24.08	6	0.69	1.84	24.89	176	0.48	1.93	26.58	143	0.20	1.87	27.56	93	0.39
1.76	24.48	6	0.70	1.89	25.14	176	0.48	1.97	26.71	143	0.22	1.90	27.81	95	0.44
1.83	24.73	6	0.69	1.94	25.28	176	0.48	2.02	26.98	143	0.24	1.93	28.76	97	0.49
1.89	24.95	6	0.66	1.99	25.54	176	0.48					1.98	28.00	97	0.50
1.94	24.98	6	0.66												
1.99	25.16	6	0.66												
2.04	25.21	6	0.66												
2.09	25.53	6	0.66												
2.14	25.48	6	0.66												
2.17	25.60	6	0.66												

TABLE 4—Continued

A2589				A2666				A2670				MKWS			
FWHM of PSF 2.3				FWHM of PSF 2.6				FWHM of PSF 2.8				FWHM of PSF 3.6			
Log r	$\mu_V$	PA	E	Log r	$\mu_V$	PA	E	Log r	$\mu_V$	PA	E	Log r	$\mu_V$	PA	E
(arcsec)				(arcsec)				(arcsec)				(arcsec)			
-0.23	18.87	0	0.14	-0.40	18.06	6	0.77	-0.36	18.39	155	0.06	-0.37	18.63	93	0.15
-0.09	19.04	0	0.14	-0.25	18.14	6	0.77	-0.21	19.46	155	0.06	-0.22	18.74	93	0.15
0.20	19.41	0	0.14	0.05	18.30	49	0.20	0.09	19.67	155	0.06	0.08	18.85	93	0.15
0.39	19.87	0	0.14	0.23	18.53	46	0.00	0.26	19.96	155	0.06	0.26	19.04	93	0.15
0.50	20.33	0	0.15	0.35	18.78	67	0.18	0.39	20.34	155	0.06	0.38	19.24	93	0.15
0.61	20.54	0	0.15	0.45	19.02	67	0.18	0.49	20.68	155	0.06	0.48	19.52	93	0.15
0.68	20.61	0	0.16	0.53	19.27	67	0.20	0.57	20.95	155	0.06	0.56	19.76	93	0.15
0.74	21.02	0	0.16	0.60	19.49	66	0.20	0.63	21.17	155	0.06	0.63	19.96	93	0.15
0.80	21.19	0	0.17	0.65	19.71	65	0.20	0.69	21.37	155	0.06	0.68	20.13	93	0.15
0.86	21.37	0	0.17	0.70	19.87	65	0.21	0.74	21.56	155	0.06	0.73	20.29	93	0.15
0.89	21.51	0	0.17	0.75	20.01	64	0.23	0.79	21.72	155	0.06	0.78	20.44	93	0.15
0.95	21.68	0	0.18	0.81	20.24	64	0.23	0.85	21.98	155	0.06	0.84	20.65	93	0.15
1.02	21.92	0	0.19	0.88	20.52	63	0.23	0.92	22.24	155	0.06	0.91	20.91	93	0.15
1.09	22.11	1	0.20	0.94	20.76	63	0.24	0.98	22.47	155	0.06	0.97	21.15	93	0.15
1.14	22.27	1	0.20	0.99	20.96	63	0.24	1.03	22.63	155	0.06	1.02	21.39	93	0.15
1.18	22.44	1	0.21	1.04	21.13	63	0.24	1.08	22.78	155	0.06	1.07	21.61	93	0.15
1.22	22.58	1	0.22	1.09	21.34	63	0.24	1.13	22.94	155	0.06	1.12	21.82	93	0.15
1.27	22.76	1	0.24	1.14	21.54	63	0.24	1.18	23.15	155	0.06	1.18	22.06	93	0.15
1.32	22.90	2	0.25	1.19	21.73	63	0.24	1.23	23.32	155	0.06	1.23	22.26	93	0.15
1.36	23.05	2	0.26	1.23	21.90	63	0.25	1.28	23.48	155	0.06	1.27	22.42	93	0.15
1.40	23.19	2	0.28	1.28	22.08	63	0.25	1.32	23.68	155	0.06	1.32	22.61	93	0.15
1.44	23.37	2	0.30	1.33	22.26	63	0.25	1.37	23.92	155	0.06	1.36	22.81	93	0.15
1.48	23.51	3	0.32	1.37	22.45	63	0.25	1.42	24.14	155	0.06	1.41	23.03	93	0.15
1.53	23.68	3	0.34	1.43	22.68	63	0.26	1.47	24.42	155	0.06	1.47	23.25	93	0.15
1.57	23.81	4	0.37	1.48	22.92	62	0.26	1.53	24.75	155	0.06	1.52	23.55	93	0.15
1.62	23.95	4	0.41	1.53	23.20	62	0.27	1.58	25.03	155	0.06	1.57	23.89	93	0.15
1.65	24.08	5	0.44	1.58	23.46	62	0.28	1.64	25.26	155	0.06	1.63	24.14	93	0.15
1.69	24.21	6	0.48	1.63	23.70	62	0.29	1.68	25.45	155	0.06	1.68	24.39	93	0.15
1.72	24.31	6	0.52	1.68	23.89	62	0.29	1.73	25.73	155	0.06	1.72	24.75	93	0.15
1.75	24.39	7	0.56	1.72	24.12	61	0.30	1.78	25.74	155	0.06	1.77	25.11	93	0.15
1.78	24.54	8	0.59	1.77	24.35	61	0.31	1.83	25.87	155	0.06	1.82	25.62	93	0.15
1.82	24.70	9	0.61	1.81	24.54	61	0.32	1.88	26.02	155	0.06	1.87	25.93	93	0.15
1.87	24.96	10	0.61	1.85	24.71	61	0.34	1.93	26.14	155	0.06	1.92	26.08	93	0.15
1.93	25.16	11	0.60	1.90	24.97	60	0.36	1.98	26.28	155	0.06	1.97	26.43	93	0.15
1.98	25.44	11	0.59	1.95	25.21	60	0.38	2.03	26.77	155	0.06	2.02	26.84	93	0.15
2.03	25.70	11	0.59	1.99	25.58	59	0.40	2.08	26.77	155	0.06	2.03	25.70	93	0.15
2.08	26.14	11	0.59	2.03	25.97	59	0.43	2.13	27.25	155	0.06				
2.13	26.32	11	0.59	2.09	26.12	59	0.43	2.18	27.61	155	0.06				
2.18	26.92	11	0.59	2.13	26.99	59	0.43	2.23	27.05	155	0.06				
2.23	27.69	11	0.59					2.27	26.86	155	0.06				

AWM1				AWM2				AWM3				AWM4			
FWHM of PSF 2.3				FWHM of PSF 3.0				FWHM of PSF 1.9				FWHM of PSF 1.6			
Log r	$\mu_V$	PA	E	Log r	$\mu_V$	PA	E	Log r	$\mu_V$	PA	E	Log r	$\mu_V$	PA	E
(arcsec)				(arcsec)				(arcsec)				(arcsec)			
0.23	18.85	74	0.21	-0.25	17.89	64	0.12	-0.26	17.45	95	0.20	-0.23	18.44	164	0.20
0.36	19.07	74	0.21	-0.09	18.01	64	0.12	-0.11	17.50	95	0.20	-0.09	18.60	168	0.13
0.45	19.36	74	0.21	0.20	18.34	64	0.12	0.20	17.94	95	0.17	0.21	18.99	168	0.13
0.53	19.62	74	0.20	0.38	18.78	65	0.13	0.36	18.42	94	0.20	0.39	19.41	168	0.13
0.60	19.86	73	0.20	0.50	19.23	65	0.13	0.48	18.87	94	0.21	0.51	19.79	168	0.13
0.66	20.07	73	0.20	0.60	19.63	65	0.13	0.58	19.23	90	0.23	0.61	20.08	168	0.13
0.71	20.25	73	0.20	0.68	19.86	65	0.13	0.66	19.55	91	0.22	0.69	20.33	168	0.14
0.75	20.42	72	0.20	0.74	20.26	65	0.13	0.73	19.83	93	0.21	0.75	20.53	168	0.14
0.82	20.65	72	0.20	0.80	20.50	65	0.13	0.79	20.07	94	0.21	0.81	20.71	168	0.14
0.89	20.93	72	0.20	0.86	20.72	65	0.13	0.84	20.29	96	0.20	0.86	20.85	168	0.14
0.95	21.18	71	0.20	0.90	20.91	65	0.13	0.89	20.48	97	0.20	0.91	20.95	168	0.14
1.00	21.40	71	0.19	0.96	21.17	65	0.13	0.95	20.71	99	0.19	0.97	21.16	168	0.14
1.05	21.61	70	0.19	1.03	21.47	65	0.14	1.02	20.99	102	0.18	1.04	21.39	168	0.15
1.10	21.83	69	0.19	1.09	21.72	65	0.14	1.08	21.20	105	0.17	1.09	21.58	168	0.15
1.16	22.05	69	0.19	1.14	21.93	66	0.14	1.14	21.44	108	0.16	1.15	21.80	168	0.15
1.21	22.24	68	0.18	1.19	22.14	66	0.14	1.19	21.63	110	0.15	1.19	22.00	168	0.16
1.26	22.41	67	0.18	1.24	22.35	66	0.15	1.24	21.85	113	0.15	1.24	22.18	168	0.16
1.30	22.59	66	0.18	1.30	22.57	66	0.15	1.30	22.16	117	0.14	1.30	22.41	168	0.17
1.35	22.78	65	0.17	1.35	22.75	66	0.15	1.35	22.42	121	0.13	1.35	22.65	168	0.17
1.40	22.98	64	0.17	1.39	22.91	67	0.16	1.40	22.64	124	0.12	1.39	22.73	168	0.18
1.45	23.24	63	0.17	1.43	23.09	67	0.16	1.45	22.91	128	0.11	1.43	22.92	168	0.19
1.51	23.52	61	0.16	1.48	23.31	67	0.17	1.50	23.14	133	0.10	1.48	23.16	168	0.19
1.57	23.80	60	0.15	1.53	23.49	68	0.17	1.55	23.36	137	0.09	1.53	23.32	168	0.20
1.62	24.05	58	0.15	1.59	23.69	68	0.18	1.60	23.54	142	0.08	1.58	23.52	168	0.21
1.67	24.30	56	0.14	1.63	23.94	68	0.19	1.66	23.84	148	0.08	1.63	23.72	168	0.23
1.72	24.58	53	0.13	1.68	24.18	69	0.20	1.71	24.32	154	0.07	1.68	24.02	168	0.25
1.77	24.76	50	0.13	1.73	24.40	70	0.21	1.77	24.55	159	0.06	1.72	24.26	168	0.27
1.82	25.04	47	0.12	1.78	24.73	70	0.22	1.82	24.73	164	0.06	1.76	24.36	168	0.29
1.87	25.22	44	0.11	1.82	25.00	71	0.24	1.86	24.53	168	0.06	1.80	24.69	168	0.31
1.92	25.44	41	0.10	1.86	25.40	72	0.25	1.91	24.73	172	0.07	1.84	25.09	168	0.35
1.97	25.77	40	0.10	1.91	25.66	73	0.27	1.96	25.12	174	0.08	1.90	25.39	168	0.39
2.02	26.34	40	0.10	1.95	25.86	74	0.30	2.00	25.55	174	0.11	1.95	25.69	168	0.44
2.07	26.49	40	0.10	1.99	26.46	75	0.33	2.04	25.57	171	0.15	2.00	26.07	168	0.50
2.12	27.03	40	0.10	2.03	27.09	76	0.35	2.08	25.50	168	0.19	2.05	26.29	168	0.56
2.16	27.32	40	0.10	2.08	27.68	76	0.35	2.13	25.26	168	0.20				
								2.18	25.44	168	0.20				
								2.23	26.14	168	0.20				

## DYNAMICS OF LUMINOUS GALAXIES

TABLE 4—Continued

AWM5				AWM6				AWM7			
FWHM of PSF 2.1				FWHM of PSF 2.2				FWHM of PSF 2.8			
Log r	$\mu_V$	PA	E	Log r	$\mu_V$	PA	E	Log r	$\mu_V$	PA	E
(arcsec)				(arcsec)				(arcsec)			
-0.25	18.02	82	0.12	0.12	18.61	35	0.00	-0.36	18.77	99	0.16
-0.13	18.12	80	0.25	0.28	18.84	35	0.05	-0.22	18.83	99	0.16
0.17	18.40	80	0.25	0.40	19.14	35	0.08	0.08	18.95	172	0.10
0.34	18.76	80	0.25	0.50	19.45	35	0.09	0.26	19.14	179	0.08
0.46	19.11	80	0.25	0.57	19.71	35	0.11	0.39	19.35	0	0.08
0.56	19.40	80	0.25	0.63	19.94	35	0.13	0.48	19.56	178	0.07
0.64	19.67	80	0.25	0.69	20.12	35	0.14	0.56	19.77	1	0.07
0.71	19.91	80	0.25	0.73	20.27	35	0.17	0.63	19.94	5	0.09
0.77	20.13	80	0.25	0.77	20.42	35	0.18	0.69	20.09	7	0.08
0.82	20.33	80	0.25	0.83	20.61	35	0.18	0.74	20.23	12	0.09
0.86	20.51	80	0.25	0.90	20.84	35	0.18	0.78	20.35	10	0.09
0.92	20.73	80	0.25	0.96	21.07	35	0.18	0.84	20.50	9	0.11
0.99	20.98	80	0.25	1.01	21.28	35	0.19	0.91	20.68	6	0.12
1.06	21.20	80	0.25	1.06	21.49	35	0.19	0.97	20.82	9	0.11
1.10	21.41	80	0.25	1.11	21.70	35	0.19	1.03	20.95	5	0.09
1.15	21.58	80	0.25	1.17	21.93	35	0.19	1.08	21.07	8	0.06
1.20	21.77	80	0.25	1.22	22.12	35	0.20	1.13	21.20	7	0.04
1.27	21.99	80	0.25	1.26	22.29	35	0.20	1.19	21.34	173	0.01
1.31	22.20	80	0.25	1.30	22.44	35	0.20	1.23	21.48	122	0.02
1.35	22.38	80	0.26	1.35	22.58	35	0.21	1.28	21.62	22	0.01
1.40	22.59	80	0.26	1.40	22.73	35	0.21	1.32	21.75	44	0.05
1.45	22.79	80	0.26	1.45	22.91	35	0.22	1.37	21.87	39	0.08
1.49	22.98	80	0.26	1.50	23.12	35	0.23	1.42	22.00	13	0.05
1.55	23.19	80	0.26	1.55	23.34	35	0.24	1.47	22.14	79	0.09
1.60	23.30	80	0.26	1.60	23.58	35	0.25	1.52	22.29	61	0.15
1.65	23.63	80	0.27	1.65	23.81	35	0.26	1.57	22.46	79	0.18
1.71	23.83	80	0.27	1.69	24.09	35	0.27	1.62	22.62	81	0.22
1.76	24.06	80	0.27	1.74	24.33	35	0.29	1.67	22.81	80	0.23
1.81	24.32	80	0.27	1.78	24.55	35	0.31	1.72	23.04	76	0.19
1.85	24.58	80	0.28	1.82	24.59	35	0.33	1.77	23.26	76	0.19
1.91	24.86	80	0.28	1.86	24.89	35	0.36	1.82	23.52	76	0.19
1.95	25.16	80	0.29	1.91	25.26	35	0.38	1.87	23.79	76	0.19
2.00	25.34	80	0.29	1.96	25.62	35	0.38	1.92	24.06	76	0.19
2.05	25.68	80	0.30	2.00	25.90	35	0.38	1.97	24.19	76	0.19
2.10	25.93	80	0.30	2.05	26.25	35	0.38	2.02	24.44	76	0.19
2.15	26.16	80	0.30	2.10	26.72	35	0.38	2.07	24.88	76	0.19
2.20	26.45	80	0.30	2.15	27.69	35	0.38	2.12	25.28	76	0.19
2.25	26.67	80	0.30					2.16	25.84	76	0.19
2.30	27.04	80	0.30								
2.35	27.50	80	0.30								

tometry is good to 0.1 mag from about 17.0 mag arcsec<sup>-1</sup> to about 24.0 mag arcsec<sup>-1</sup>.

The BCM galaxies of A2147, A2162, and A2670 all have surface brightness profiles from O76. The BCM galaxies in A2147 and A2162 were observed by us in the 1982 June KPNO run, and the BCM in A2670 was observed during the 1981 December McGraw-Hill run. Likewise, the “poor cluster cD’s” in MKW 5, AWM 1, AWM 4, AWM 5, and AWM 7 were observed in the 1982 May, 1981 December, 1982 June, 1982 June, and 1981 December runs, respectively. These galaxies all have surface brightness profiles published by TR. We plot both our profile (*dots*) and either O76’s or TR’s (*plus signs*) for these eight galaxies in Figure 2. No zero-point shift has been made in these plots except for the  $V-g$  and  $V-r$  colors for the TR photometry. In those cases the colors, about  $-0.27$  and  $0.29$  mag, respectively, were taken directly from TR. This lack of a shift allows us to judge the quality of the absolute photometry from Figure 2. On the whole, the agreement with these other authors is quite good except for the BCM galaxy in AWM 5 where the TR profile falls off more rapidly than ours does. Similar deviations are seen in A2162 and AWM 1, but in these two galaxies the deviations start at a surface brightness of about 24.0 mag arcsec<sup>-2</sup> and are probably due to uncertainty in the sky level. In AWM 5 the deviation starts at about 21.0 mag arcsec<sup>-2</sup> and cannot be due to the sky value. The only conclusion seems to be that either TR’s photometry or ours is wrong for this galaxy.

Our photometry disagrees slightly with that of the other

authors in a few other respects. There is a small deviation in our profile of A2147 at  $\log r \approx 1.6$ . Since we had only one 5 minute exposure of this galaxy, an attempt was made to extend the photometry to larger radii than was normally done with a short exposure. However, this resulted in a ragged profile at large radii. We conclude that the disagreement is due to poor signal-to-noise ratio in our data in this case.

Our profile of A2670 is somewhat lower in surface brightness in the 1”–8” range than O76’s. Dressler (1978) also finds that O76’s surface brightness is too high in the same radius range in this galaxy.

The comparison of all of these galaxies with the O76 and TR photometry gives us confidence that both our absolute and our relative photometry are satisfactory. We estimate that the errors are no larger than 0.1 mag down to a surface brightness of about 25 mag arcsec<sup>-2</sup>. The errors increase after that as a result of difficulty in the determination of the sky level, and not because of low signal-to-noise ratio except in the few cases when only one short (5 minute) exposure was obtained (see Fig. 3).

Examination of Figure 2 also serves to illustrate the relative advantages and disadvantages of using a CCD camera to do surface photometry. Our profiles extend only to a radius of about 100”–150”. This is true even though the O76 and TR profiles, based on photoelectrically calibrated photography, show that there is galaxy light much farther out. Measurements at large radii from the center of the galaxy are difficult because of the small size of the CCD chip. On the other hand,

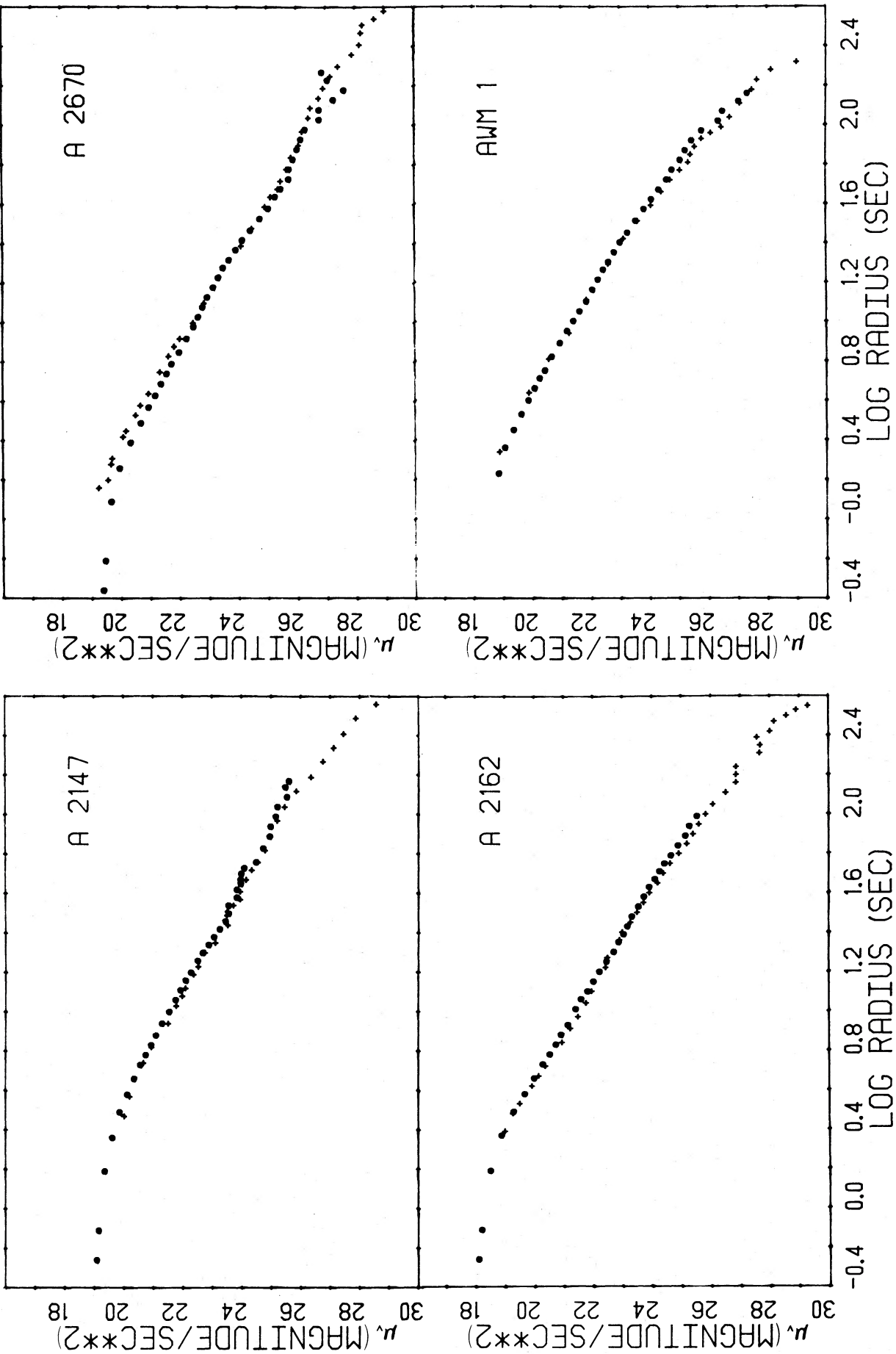


FIG. 2.—Comparison of surface brightness profiles of three galaxies in common with Oemler (1976) (A2147, A2162, and A2670) and five in common with Thuan and Romanishin (1981) (AWM 1, AWM 4, AWM 5, AWM 7, and MKW 5). Our photometry is displayed by dots, and the other authors' is displayed by plus signs. Note that no zero-point shift has been made except for the  $V - g$  and  $V - r$  colors for the Thuan and Romanishin (1981) profiles.

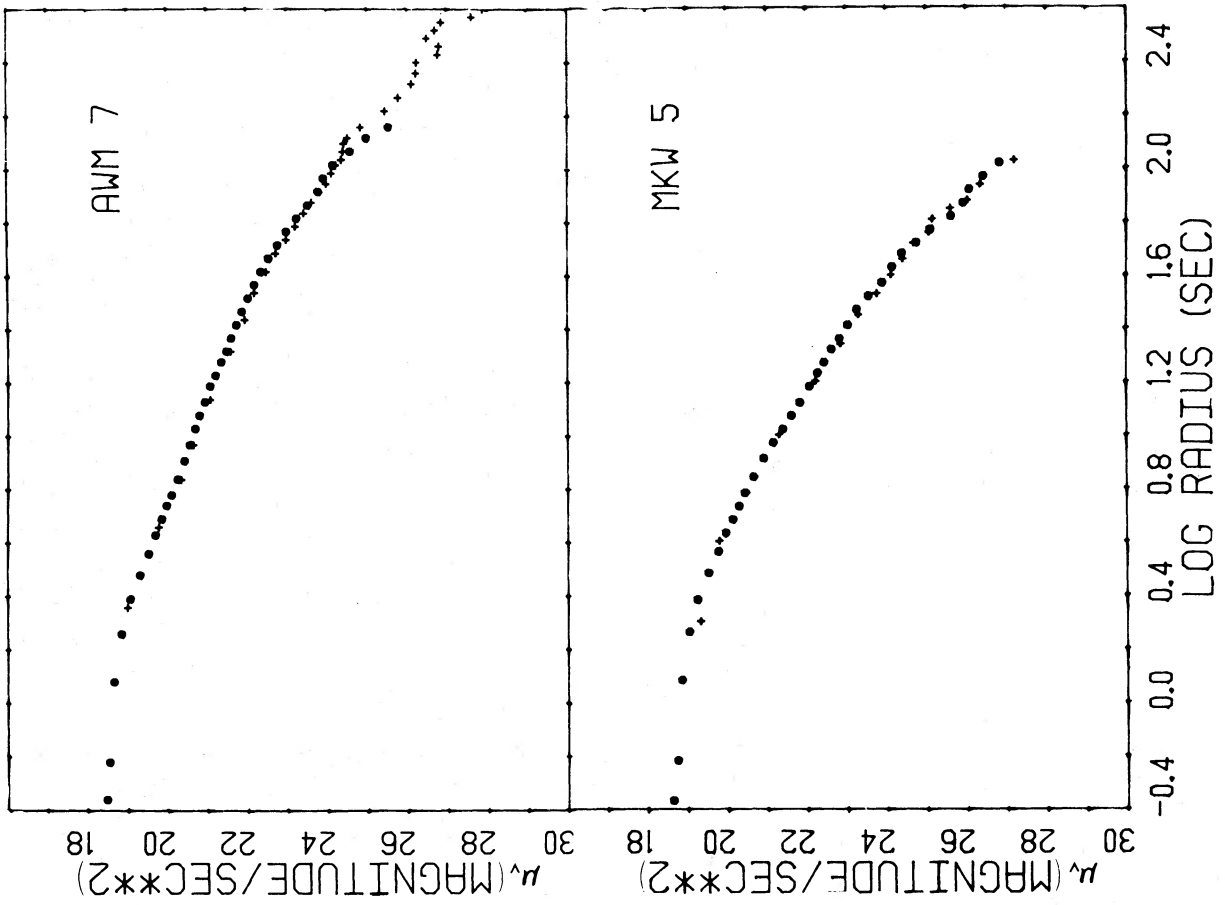


FIG. 2.—Continued

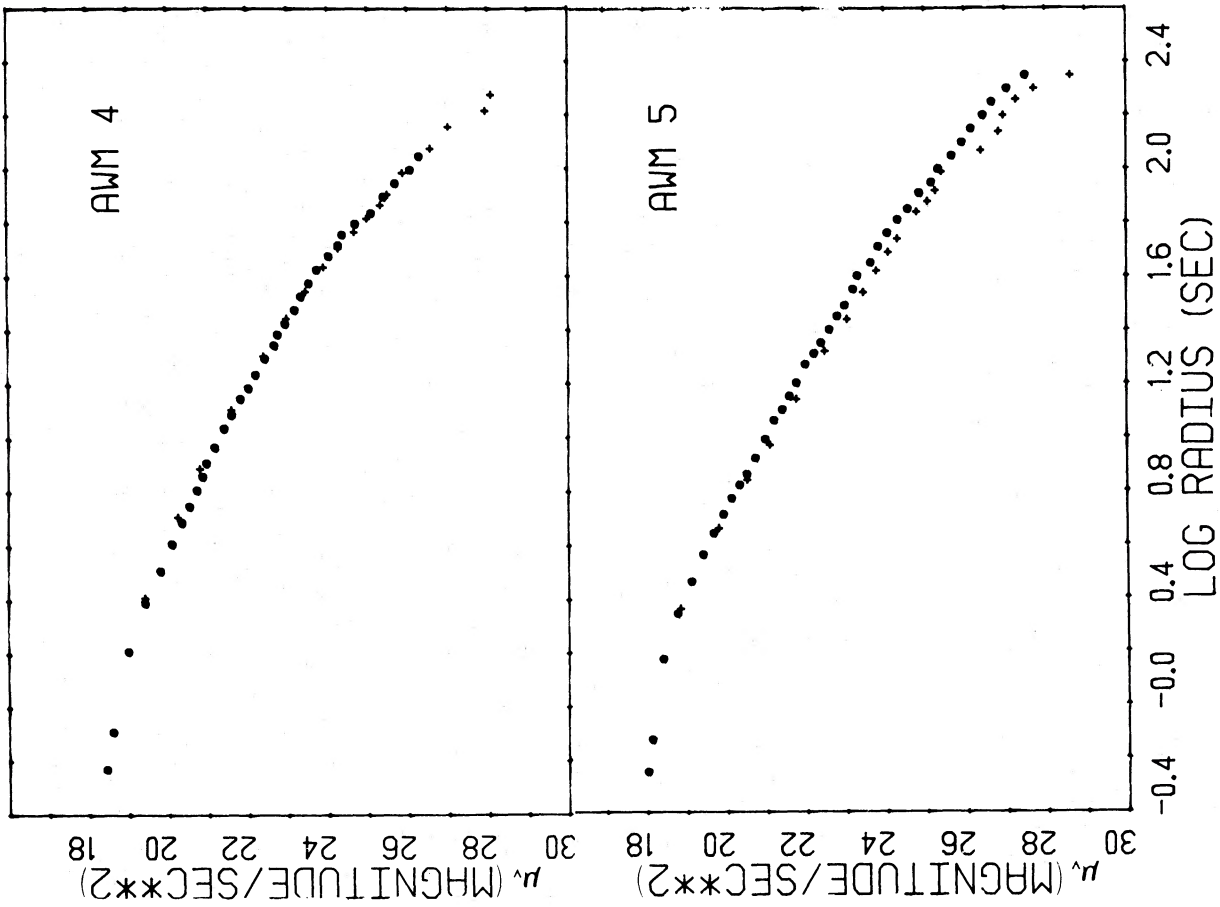


FIG. 2.—Continued

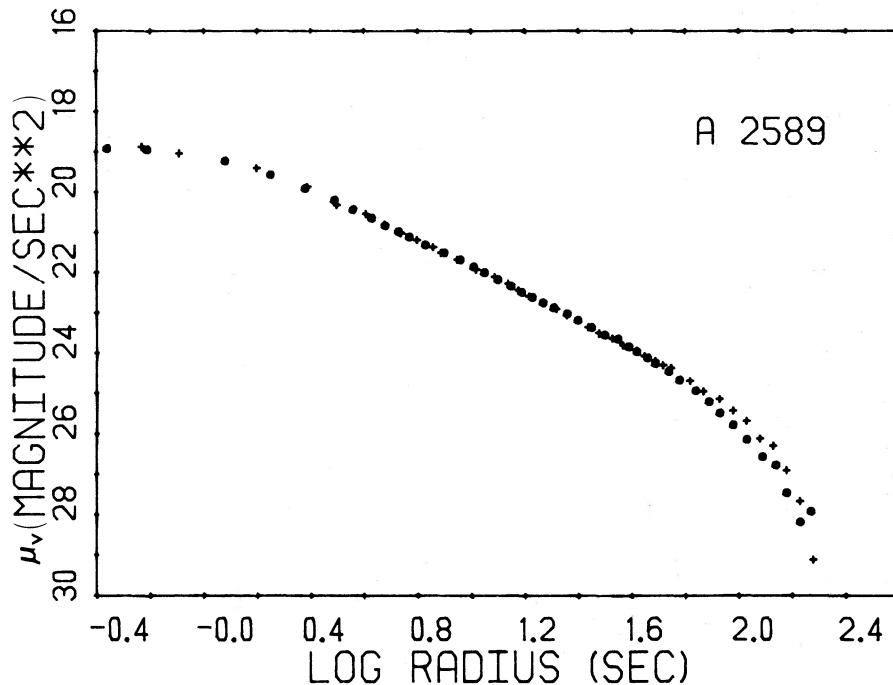


FIG. 3.—Surface brightness profiles of A2589 from the McGraw-Hill data (dots) and from the KPNO data (plus signs). No zero-point shift has been made. The agreement is very good (better than 0.03 mag) from  $\log r = 0.7$  to  $\log r = 1.5$  ( $5''$ – $34''$ ) and is good (better than 0.1 mag) from  $\log r = -0.2$  to  $\log r = 1.7$  ( $0''.6$ – $52''$ ).

the photographic photometry of O76 and TR contains no information at radii less than  $2''$ – $2''.5$  from the center, while we often obtain information, to within the limits of seeing, inside the central arcsecond. It should be remembered that because of the small field of the CCD the “total” magnitudes in this paper may be too faint for the most extended of the galaxies. In the worst case the total magnitude derived from the photometry of AWM 7 in this paper is 0.74 mag fainter than TR’s value. AWM 7 is one of the closest galaxies and is the most extended BCM galaxy in this sample. The total magnitudes of A2147, A2162, A2670, and AWM 4 are about 0.3 mag fainter than the O76 or TR values for these galaxies. The total magnitudes of the others agree better than this. We use the total magnitudes of O76 or TR for these five galaxies in the analysis in § IV.

As a check on the consistency of the photometry between the two telescope-camera combinations used in this work, one galaxy, the BCM in A2589, was observed with both telescopes and reduced separately. Figure 3 compares the profiles. The agreement between them is good to a surface brightness about  $25 \text{ mag arcsec}^{-2}$ . The magnitude difference is less than 0.1 mag in the range from  $0''.6$  to  $52''$  ( $19.0$ – $24.3 \text{ mag arcsec}^{-2}$ ), and less than 0.17 mag (peak to peak) out to a radius of  $74''$  (about  $25 \text{ mag arcsec}^{-2}$ ). The agreement is very good (better than 0.03 mag) in the  $5''$ – $34''$  range ( $20.8$ – $23.7 \text{ mag arcsec}^{-2}$ ). After that, uncertainty in the sky leads to a larger disagreement between the two profiles (0.5 mag at  $135''$ , or about  $26.5 \text{ mag arcsec}^{-2}$ ). Again this comparison gives us confidence in our absolute and relative photometry, and a knowledge of its limits.

#### d) The Luminosity Distribution of BCM Galaxies

One interesting result of Paper I was that the seven BCM galaxies showed a higher central mass-to-light ratio than the elliptical galaxies. To determine these core mass-to-light ratios we require an estimate of the central density (King and Minkowski 1972; FJ; S80). King (1966) models were used to

characterize the luminosity distribution of the O76 BCM galaxies, since these models offer a simple way to estimate the central density. While seeing effects make it hard to determine the core radius,  $R_c$ , and the central surface brightness,  $I_0$  (Schweizer 1979), it is the product  $I_0 R_c$  which is important in determining  $M/L$ , and this product is less affected by seeing than is either parameter alone (S80; see also Paper I, eq. [5]).

We attempted to fit a King (1966) model to each of the galaxies observed here, taking the seeing into account. An estimate of the seeing was made for each frame by looking at the light distribution of a star in the field. The luminosity distribution of this star is the point spread function (PSF) of that frame. The full width at half-maximum (FWHM) of the PSF is given for each galaxy in Table 4. Following Schweizer (1979), we convolved the PSF with the King (1966) model and fitted the convolved model to the luminosity profile of the galaxy. Since the King (1966) model is dimensionless, a core radius,  $R_c$ , and central surface brightness,  $I_0$ , were assumed before the convolution was done. The convolved model was then plotted with the data. The distance between the model and the data along each axis was used to make a better guess of the values of  $R_c$  and  $I_0$ . The process was repeated until a satisfactory fit was obtained. Of the 27 BCM galaxies observed in this paper, 15 were fitted well from the center out to a surface brightness of about  $24 \text{ mag arcsec}^{-2}$  by the seeing-convolved King (1966) models, while six others (A505, A1631, A2029, A2107, A2589, and MKW 5) could be fitted approximately. That leaves six (A401, A496, A2052, A2124, AWM 4, and AWM 7) for which no satisfactory fit could be obtained. These galaxies have smaller cores than the other galaxies, and have a shallower falloff of their light with radius than all but three of the other galaxies. The surface brightness of the BCM in AWM 7 falls as  $r^{-1.05}$  over a range of  $4''$ – $40''$ , as compared with the  $r^{-2}$  profile of the Hubble law (Hubble 1930)! The parameters of the King (1966) model fits are given in Table 5. The surface bright-

TABLE 5  
PARAMETERS OF FITS TO THE SURFACE PHOTOMETRY OF BCM GALAXIES

Cluster	$\sigma$	$M_v$	$R_c$ (kpc)	$I_0$ (mag arcsec <sup>-2</sup> )	$R_e$ (kpc)	$I_e$ (mag arcsec <sup>-2</sup> )	$M_{vK}$	$M_{vd}$	$M/L$ ( $M_\odot/L_{v\odot}$ )
A150	245	-24.43	3.26	19.25	48.22	24.35	-24.17	-24.04	6.7
A401	367	-24.33	...	...	91.04	25.29	...	-24.48	...
A496	254	-24.16	...	...	59.65	24.51	...	-24.35	...
A505	408	-24.65	3.41	18.80	38.52	23.45	-24.52	-24.43	12.0
A779 <sup>a</sup>	372	-23.65	1.75	18.00	19.95	22.79	-23.58	-23.69	10.0
A994	330	-23.30	1.11	17.35	11.41	21.98	-23.34	-23.25	6.7
A1177	279	-24.03	0.70	17.00	23.30	23.09	-23.97	-23.73	5.7
A1631	249	-22.53	0.73	17.70	12.32	22.77	-22.48	-22.66	8.9
A1904	...	-24.40	2.84	18.50	37.61	23.55	-24.49	-24.30	...
A2029	375 <sup>b</sup>	-25.40	6.18	19.42	84.44	24.34	-25.47	-25.26	9.1
A2052	197	-24.30	...	...	77.54	24.73	...	-24.70	...
A2107	438	-24.31	2.66	18.65	42.17	23.77	-24.34	-24.32	15.9
A2124	...	-24.32	...	...	37.53	23.56	...	-24.27	...
A2147	306	-24.57 <sup>c</sup>	2.36	18.70	34.60	23.73	-24.23	-23.93	9.5
A2162	342	-23.95 <sup>c</sup>	1.23	17.35	16.44	22.42	-23.66	-23.64	6.7
A2199 <sup>a</sup>	380 <sup>d</sup>	-24.89	5.20	19.30	50.15	23.92	-24.28	-24.56	10.1
A2366	391	-24.25	1.70	17.79	23.66	22.94	-24.03	-23.89	8.6
A2457	477	-23.83	2.63	18.67	23.23	23.10	-23.81	-23.71	18.4
A2589	346	-24.32	1.38	18.00	45.70	24.19	-24.30	-24.09	10.7
A2634 <sup>e</sup>	397	-24.50	...	...	...	...	...	...	...
A2666	363	-23.81	1.20	17.45	19.13	22.64	-23.80	-23.74	8.7
A2670	426	-25.23 <sup>c</sup>	2.40	18.55	50.66	24.12	-24.55	-24.37	13.5
Virgo (M87) <sup>a</sup>	343 <sup>f</sup>	-23.53	1.60	17.60	11.90	21.90	-23.34	-23.46	6.3
MKW 2 <sup>g</sup>	416	-24.29 <sup>h</sup>	2.64	18.40	30.44	23.18	-24.24	-24.20	11.8
MKW 4 <sup>i</sup>	243	-23.96	3.35	18.87	32.90	23.28	-24.27	-24.29	5.3
MKW 5	364	-23.10	1.12	17.85	17.19	22.93	-23.07	-23.21	13.5
MKW 1s <sup>g</sup>	206	-22.83	...	...	17.33	23.31	...	-22.80	...
AWM 1	213	-23.43	1.51	18.05	18.31	22.94	-23.39	-23.33	4.1
AWM 2	247	-23.08	0.72	17.05	10.32	22.10	-22.89	-22.95	4.7
AWM 3	328	-22.83	0.50	16.65	7.12	21.80	-22.45	-22.44	8.6
AWM 4	278	-23.95 <sup>j</sup>	...	...	37.39	23.76	...	-24.08	...
AWM 5	228	-24.63	2.02	17.80	30.88	23.01	-24.49	-24.41	2.7
AWM 6	327	-24.24	1.63	17.80	29.88	23.16	-24.23	-24.18	6.9
AWM 7	335	-24.68 <sup>j</sup>	...	...	70.80	24.58	...	-24.65	...

<sup>a</sup> Surface photometry from Oemler 1976.

<sup>b</sup> Velocity dispersion from Dressler 1979.

<sup>c</sup> Surface photometry from this paper; total magnitude from Oemler 1976.

<sup>d</sup> Velocity dispersion is a weighted average between Faber and Jackson 1976 (weight 2) and this paper (weight 1).

<sup>e</sup> Total magnitude from Oemler 1976; surface photometry not available.

<sup>f</sup> Velocity dispersion is the average of three values in this paper.

<sup>g</sup> Surface photometry from Thuan and Romanishin 1981.

<sup>h</sup> The total magnitude from Thuan and Romanishin 1981 corrected for some confusion between the redshifts of MKW 2 and MKW 2s in Schild and Davis 1979.

<sup>i</sup> Surface photometry from Oemler 1976, with zero-point correction from Thuan and Romanishin 1981.

<sup>j</sup> Surface photometry from this paper; total magnitude from Thuan and Romanishin 1981.

ness profiles of all 27 BCM galaxies are shown in Figure 4. The best-fitting seeing-convolved King (1966) model is also drawn on these plots, except for the six galaxies which could not be fitted.

Each galaxy was also fitted to an  $R^{1/4}$  law (de Vaucouleurs 1958) between 1 and 25 core radii. The six galaxies which were not fitted by King (1966) models were fitted between  $2''$  and  $50''$ . This range avoids both the inner region, which is affected by seeing, and the outer region, which is affected by the presence of an envelope in some of the galaxies. The effective radius,  $R_e$ , and the surface brightness at the effective radius,  $I_e$ , are also listed in Table 5, along with the velocity dispersion, absolute magnitude, absolute magnitude of the King (1966) model ( $M_{vK}$ ), absolute magnitude of the de Vaucouleurs  $R^{1/4}$  law ( $M_{vd}$ ), and the derived core mass-to-light ratio, for each galaxy. Note that some of these galaxies have luminous envelopes (A2670, for example); in those cases  $M_{vK}$  and  $M_{vd}$  are smaller than  $M_v$  and represent the magnitude of the galaxy without its envelope. We discuss the mass-to-light ratios in §

IVd. The absolute magnitudes in this table are from integrating under the data obtained here, except where the O76 or TR photometry shows that there is more light beyond the last isophote measured here. In those cases the O76 or TR magnitudes are listed in Table 5.

#### IV. DISCUSSION

##### a) $L$ versus $\sigma$ for BCM Galaxies

We showed in Paper I that the eight BCM galaxies in that sample were brighter than predicted by the  $L \propto \sigma^4$  relation for elliptical galaxies. The chief reason for making the observations described in this paper was to see whether this conclusion persists with a larger sample of BCM galaxies.

Table 6 lists 29 elliptical galaxies with velocity dispersions from this work or from WK. The five galaxies from WK were observed with the same telescope and instrument in a manner almost identical with those observed in this work. The magnitudes for the E galaxies are taken from either the *Second Refer-*

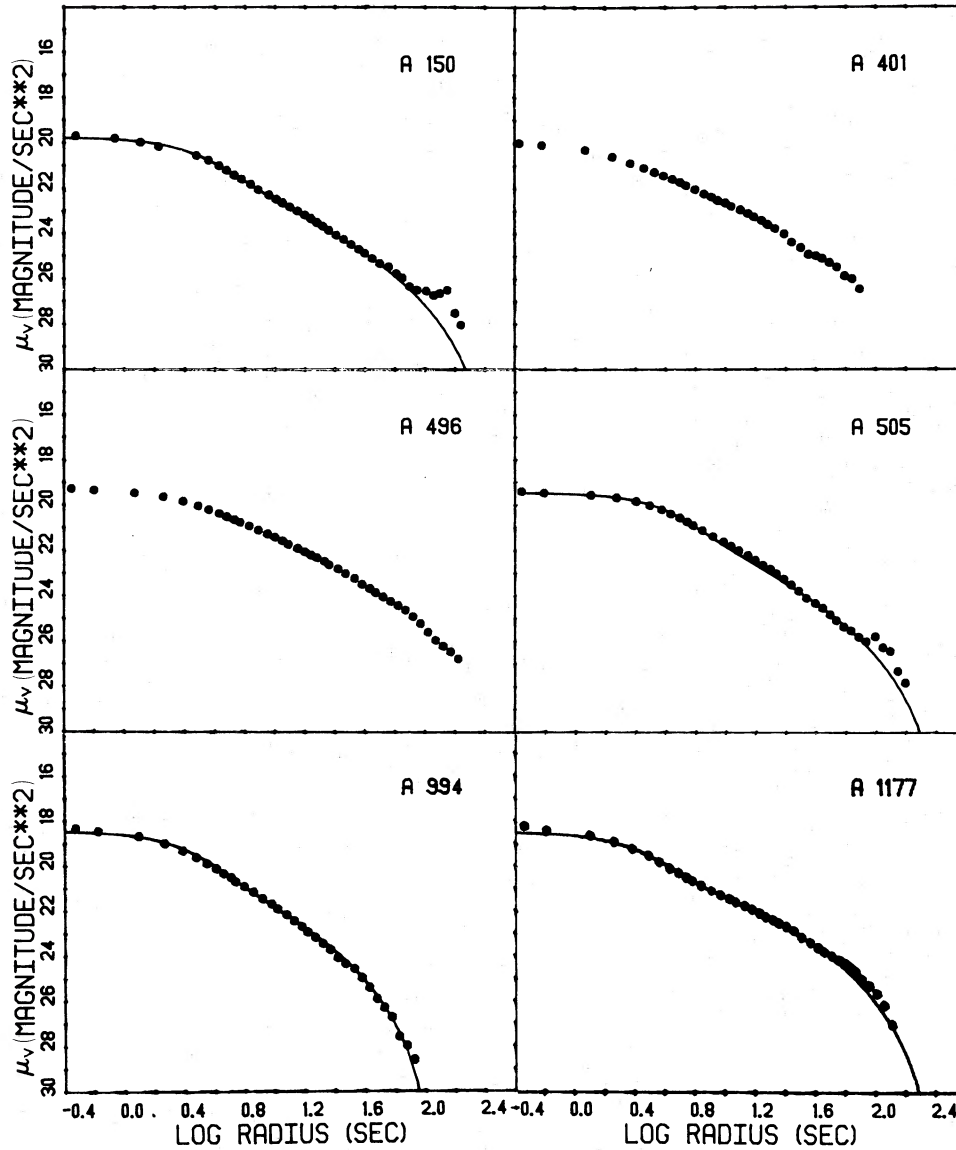


FIG. 4.—Surface brightness profile of all 27 BCM galaxies. The best fitting King (1966) model is also plotted for each galaxy, except for the six which could not be fitted well.

ence *Catalogue of Bright Galaxies* (de Vaucouleurs, de Vaucouleurs, and Corwin 1976, hereafter RC2) or O76. Comparison of eight elliptical galaxies in O76 with the magnitudes in the RC2 shows no significant differences for elliptical galaxies. As shown earlier, the photometry in this paper agrees well with that of O76 for BCM galaxies, except that our photometry does not go as far out in some of the galaxies.

A fit of  $\log \sigma$  versus  $M_v$  was made for these 29 E galaxies. A mean relation of the form  $L \propto \sigma^{4.37 \pm 0.43}$  was obtained from doing the regression both ways. Since this is not significantly different from  $L \propto \sigma^4$ , we constrain the slope to be 0.1 in the  $\log \sigma - M_v$  relation. The best fitting line in the  $\log \sigma - M_v$  plane is

$$\log \sigma = 0.177 - 0.1M_v. \quad (1)$$

This gives a magnitude at  $\sigma = 300 \text{ km s}^{-1}$  of  $M_v(300) = -23.00$ .

We plot the velocity dispersion against the absolute magnitude for all of the galaxies in Figure 5. The filled circles are the

29 E galaxies, while the open symbols are the BCM galaxies. The line is the fit given in equation (1). Of the BCM galaxies, a subset of 18 have been classified as cD galaxies by Morgan and his coworkers (Matthews, Morgan, and Schmidt 1964; Morgan and Lesh 1965; MKW; AWM; Bautz and Morgan 1970). From here on we will refer to this subset as the "Morgan cD's." The Morgan cD's are indicated in Table 7. This is not to say that the other BCM galaxies would not be called cD's by Morgan, but only that they were not so classified in one of these papers. The Morgan cD's are plotted in Figure 5 as open squares.

Inspection of Figure 5 shows that while some of the BCM galaxies are far from the line, others lie along the extension of equation (1) to larger luminosity. The elliptical galaxies and many of the BCM galaxies may be consistent with a somewhat steeper slope to the luminosity-velocity dispersion relation than  $L \propto \sigma^4$ . However, if we restrict ourselves to the range of velocity dispersions where there is overlap between the E and

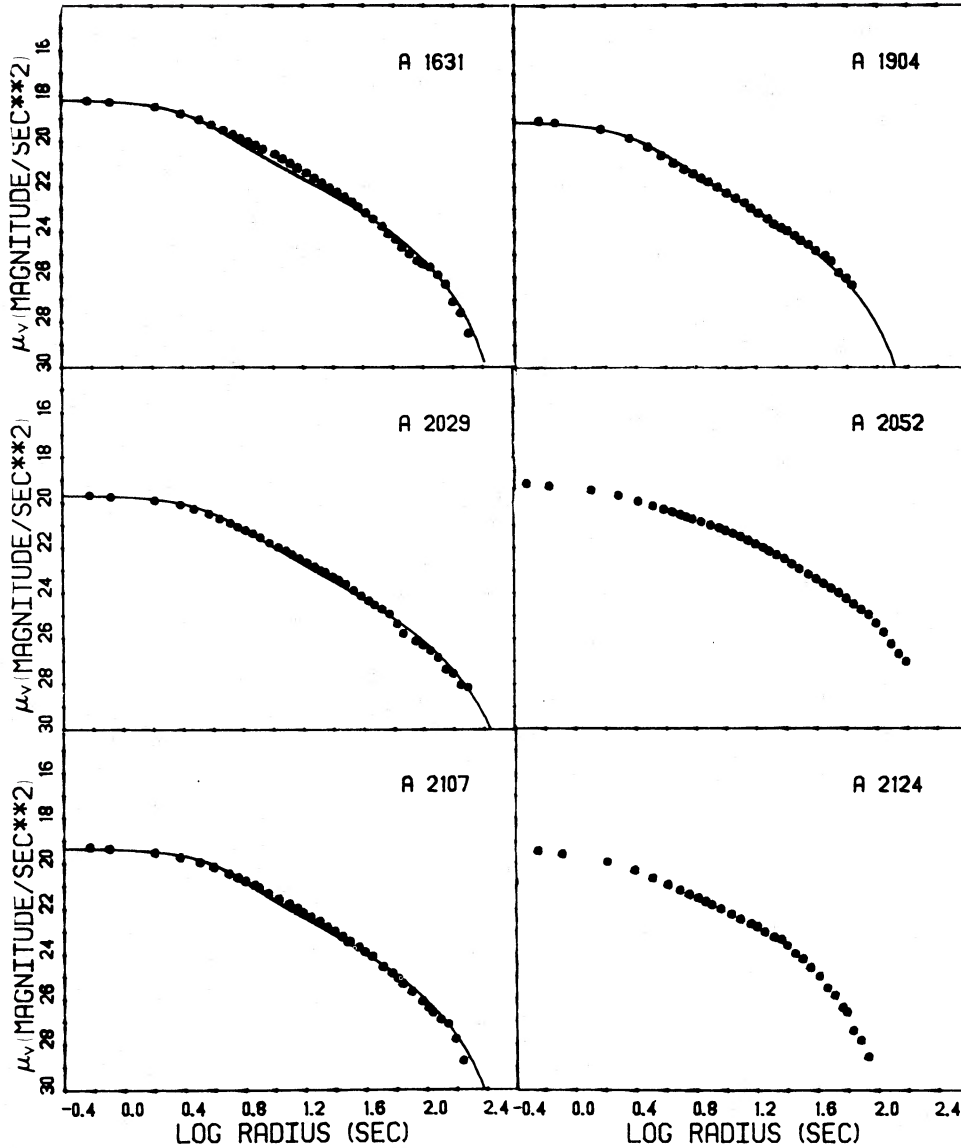


FIG. 4.—Continued

BCM galaxies, we see that the BCM galaxies average 1.22 mag brighter. This is true even though the average velocity dispersions are almost the same ( $279 \text{ km s}^{-1}$  for the 19 BCM galaxies and  $277 \text{ km s}^{-1}$  for the 21 E galaxies in the range  $193 \text{ km s}^{-1} \leq \sigma \leq 346 \text{ km s}^{-1}$ ). Histograms of the magnitudes of the E galaxies and the BCM galaxies in this range of velocity dispersion are shown in Figure 6. It is clear that no matter what the relation is between luminosity and velocity dispersion, where there is overlap the BCM galaxies are more luminous than the E galaxies of the same velocity dispersion. It is interesting to note that if the BCM galaxies alone were plotted in Figure 5, there would be only a weak relation between  $L$  and  $\sigma$ . The velocity dispersion is a poor predictor of the luminosity of a BCM galaxy. The reader should also bear in mind that since this is a log-log plot, equal residuals in  $L$  and  $\sigma$  will appear to be smaller near the upper right-hand corner of Figure 5 than in the middle of the plot.

In Figure 7 we plot histograms of the luminosity residuals,

$\Delta L = L_v - L_\sigma$ , from equation (1) for the elliptical galaxies and the BCM galaxies. The luminosity residuals of all of the BCM galaxies are listed in Table 7. The Morgan cD subset of the BCM galaxies is shown in cross-hatching. The elliptical galaxies have small residuals in  $L$ , and the distribution is symmetric about zero. The BCM galaxies, however, are scattered in a flat distribution with most (23 of 32) galaxies having positive residuals. The Morgan cD subset of the BCM galaxies have an even higher percentage of positive residuals. Fifteen of the 18 Morgan cD's have positive residuals. That leaves eight of the 14 other BCM galaxies with positive residuals. Fourteen of the BCM galaxies have positive residuals greater than  $2 \times 10^{11} L_\odot$ , while only one has a negative residual of that size. Of those 14 galaxies, 10 are Morgan cD's.

The location of most BCM galaxies to the right of the  $L-\sigma^4$  line in Figure 5 presents an interesting question for interpretation. It might have its origin in the selection of the sample. For example, if galaxies of a given  $\sigma$  have a range in  $M$ , then

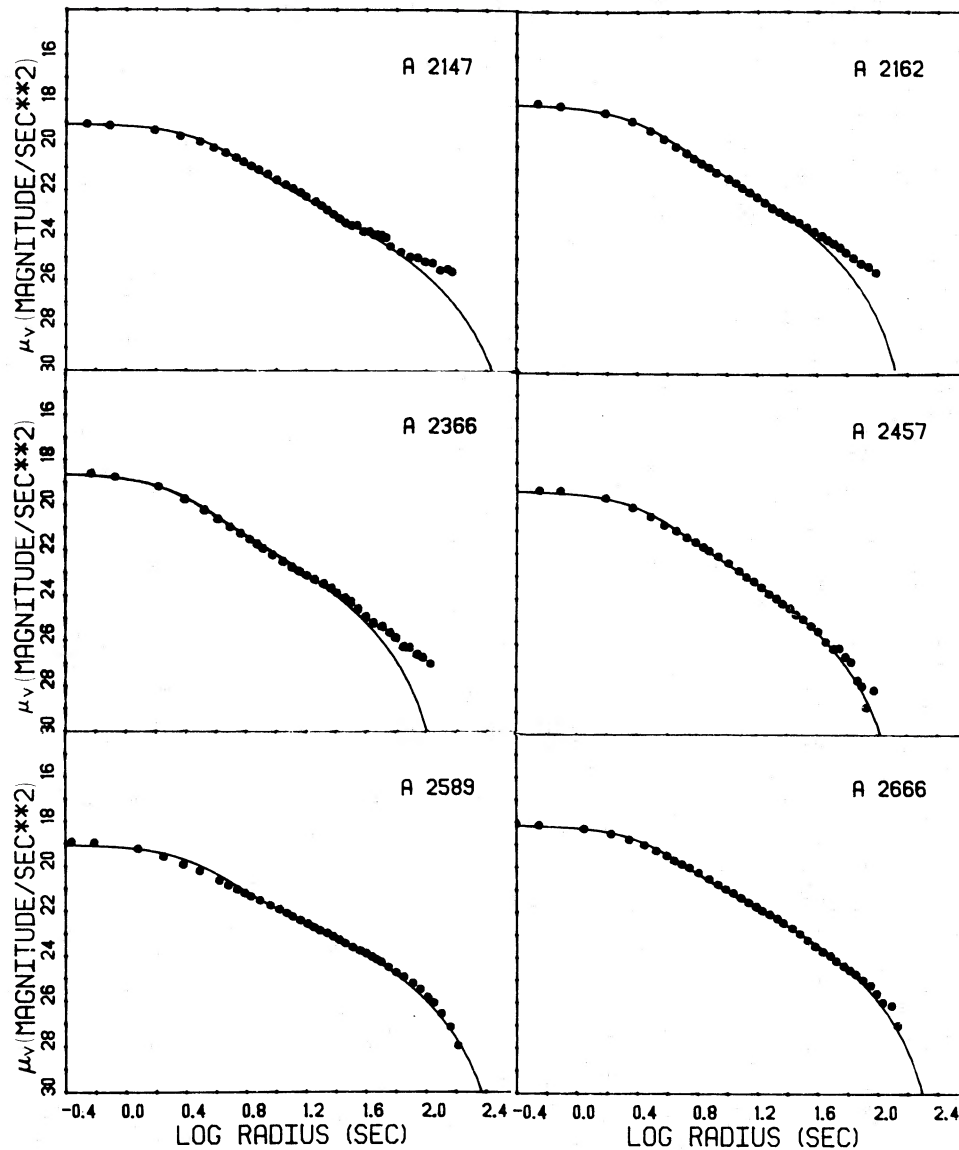


FIG. 4.—Continued

picking the brightest galaxies in a cluster will select galaxies with unusually large  $M$  for that velocity dispersion. We explore this possibility in § IVb. Alternatively, the simplest picture of galaxy mergers predicts that galaxies grow in luminosity at constant velocity dispersion. This could also produce the effect demonstrated in Figure 5. We examine the merger picture in § IVc.

#### b) A Selection Model for the $\Delta L$ Relation

One interpretation of Figure 5 might be to treat the velocity dispersion  $\sigma$  as the independent variable. Then, at any value of  $\sigma$ , you expect to find some mean value of absolute magnitude,  $\bar{M}$ , with some scatter about the mean. Then in a cluster, the brightest galaxy will most likely be one that deviates from the mean  $M$ - $\sigma$  relation and could produce an effect with the sense of that seen in Figure 5: BCM galaxies would be especially luminous in relation to their velocity dispersions.

To evaluate the effect, we have used a statistical model for a

cluster. We start with the assumption that  $L \propto \sigma^4$  and that  $\sigma$  is the independent variable. We draw 400 samples (corresponding to a zero-richness cluster like most of ours) from a distribution of  $\sigma$ 's that corresponds to Schechter's (1976) luminosity function. The low  $\sigma$  cutoff was  $85 \text{ km s}^{-1}$  (the mean absolute magnitude of a galaxy with  $\sigma = 85 \text{ km s}^{-1}$  was  $-17.50$ ), and the high  $\sigma$  cutoff was  $560 \text{ km s}^{-1}$ ; however, few galaxies had velocity dispersions above  $450 \text{ km s}^{-1}$  ( $M_p = -24.8$ ). We include the scatter about the  $L \propto \sigma^4$  line as derived from our own observations of elliptical galaxies: as shown in Figure 7, the scatter is well approximated by a Gaussian, with a Gaussian width of 0.76 mag. Then we can find the brightest galaxy in each sample cluster and compute  $\Delta L = L - L(\sigma)$ . We have run this simple simulation 150 times to obtain the distribution of  $\Delta L$  shown in Figure 7.

Also shown in Figure 7 is the observed distribution of  $\Delta L$  for our sample of BCM galaxies. An application of the Kolmogorov-Smirnov test shows that the probability that the

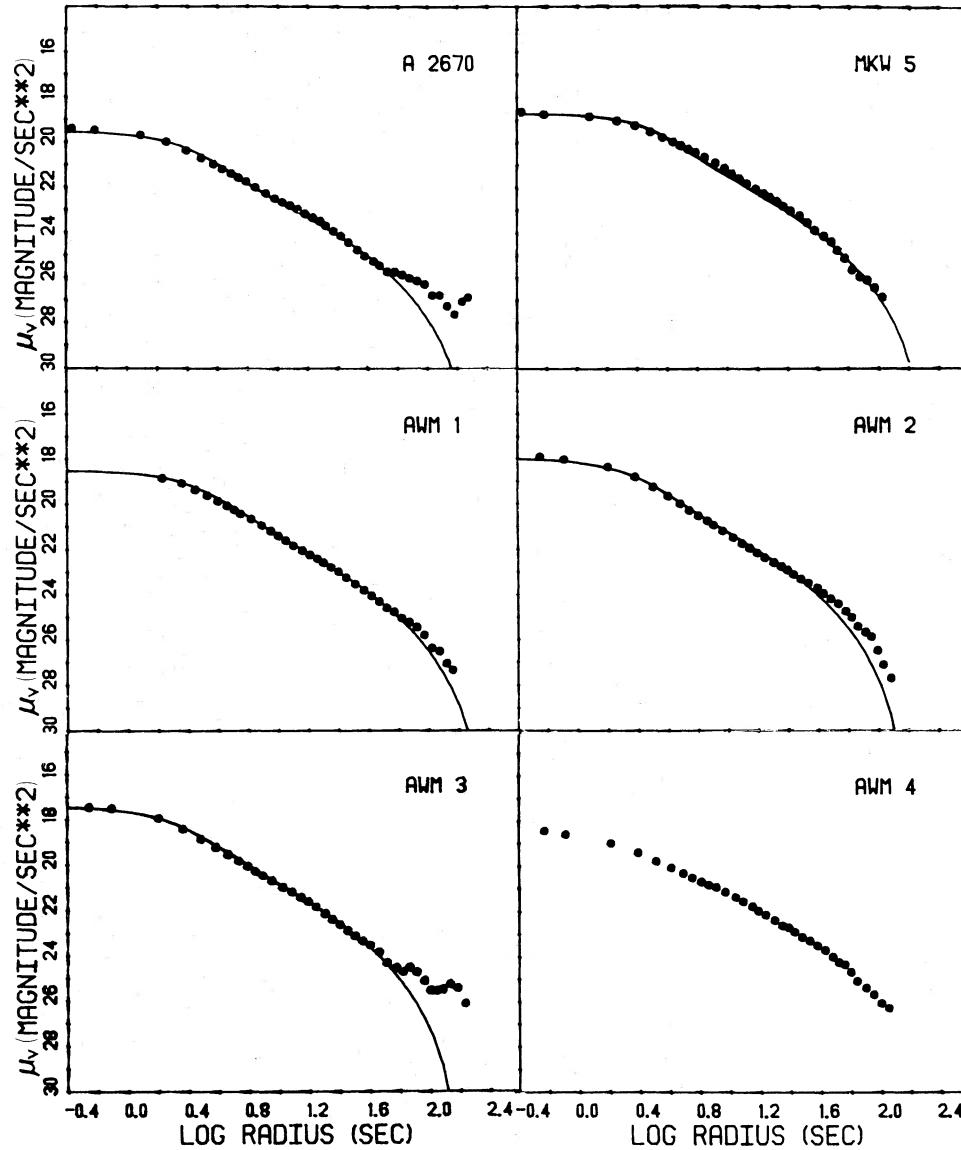


FIG. 4.—Continued

observations are *not* drawn from the population produced by the selection model is 99.9%. Inspection of the two distributions shows that while the model can account for  $\Delta L$  values as large as those seen, it does not account for the substantial number of small values of  $\Delta L$ . Too few model clusters have a brightest galaxy with  $\Delta M < 0.45$ . To be precise, 19 out of 150 model clusters have values of  $\Delta M$  as small as 0.45 mag, while 15/32 in the real sample have such modest deviations from the mean relation. This statistical model usually produces a large residual, while the observations show that small residuals are also common.

Since the elliptical galaxies used in this paper are not drawn from a volume-limited sample, it is possible that they suffer from a Malmquist bias. If the ellipticals were a magnitude-limited sample, then the mean absolute magnitude at a given velocity dispersion would be too bright by about 0.8 mag for a dispersion in  $M_b$  of 0.76. The sample of elliptical galaxies was chosen for convenience and is not magnitude-limited. The

effect must be smaller than 0.76 mag; however, it still may be significant. If we assume that selection biases the mean absolute magnitude of the elliptical galaxies to be too bright by 0.4 mag at each  $\sigma$ , the observed distribution of  $\Delta M$  values shown in Figure 7 for the BCM galaxies would be shifted 0.4 mag to the right. This would make the observed distribution more like the model distribution. Applying the Kolmogorov-Smirnov test shows that the probability that the shifted BCM galaxies are not drawn from the model distribution is only 75%. The present sample of elliptical galaxies is not well enough understood to say whether a Malmquist bias of about 0.4 mag is reasonable. A better understood sample of elliptical galaxies is necessary before we can conclude whether this simple picture in which  $\sigma$  is the independent variable and  $M$  has a spread can account for the observed distribution in  $\Delta L$ .

The fact that many of our clusters are Bautz-Morgan type I or type I-II means that we emphasize clusters where the brightest galaxy is much brighter than the second brightest.

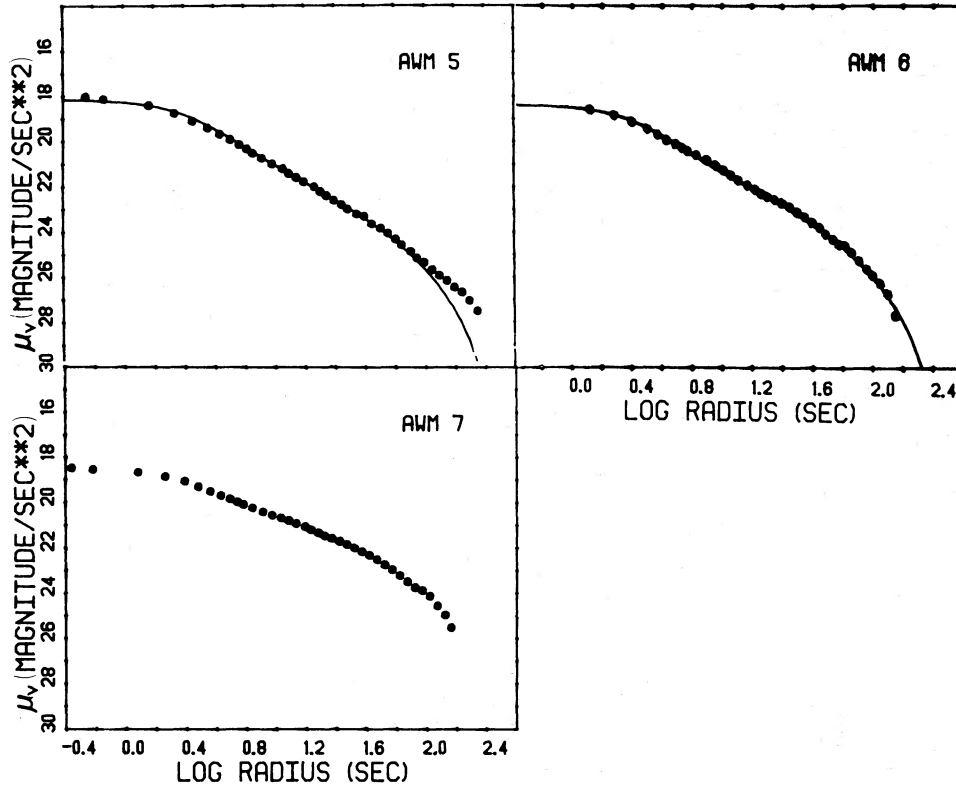


FIG. 4.—Continued

TABLE 6  
ELLIPTICAL GALAXIES

Galaxy	$\sigma$	$M_v$
NGC 533	284	-23.79
NGC 636	174	-21.68
NGC 1052	193	-21.75
NGC 1209	281	-22.27
NGC 1272	344	-22.87
NGC 1273	259	-22.29
NGC 1278	245	-23.02
NGC 1400	250	-21.05
NGC 1426	153	-20.55
NGC 1521	296	-23.12
NGC 2672	332	-23.02
NGC 2693	297	-23.24
NGC 3377	186 <sup>a</sup>	-20.64
NGC 3379	246 <sup>a</sup>	-21.59
NGC 4374	299	-22.36
NGC 4387	165 <sup>a</sup>	-19.72
NGC 4406	244	-22.52
NGC 4458	176	-19.65
NGC 4467	102	-17.23
NGC 4472	343	-23.33
NGC 4473	203	-21.55
NGC 4478	127 <sup>a</sup>	-20.50
NGC 4551	132 <sup>a</sup>	-19.83
NGC 4564	245	-20.76
NGC 4649	324	-22.87
NGC 4692	230	-23.12
NGC 4874	311	-23.83
NGC 7626	310	-22.91
IC 708	283	-23.46

<sup>a</sup> Velocity dispersion from Whitmore and Kirshner 1981.

Applying the same criterion to the simulations makes the derived distribution even *less* like the observations, since it emphasizes the cases with large  $\Delta L$ . An interesting investigation would be to observe a sample of Bautz-Morgan type III or type II-III clusters of comparable richness. In those clusters, mergers are not expected to play a major role. If there is no statistical effect of the type we have investigated here, then the

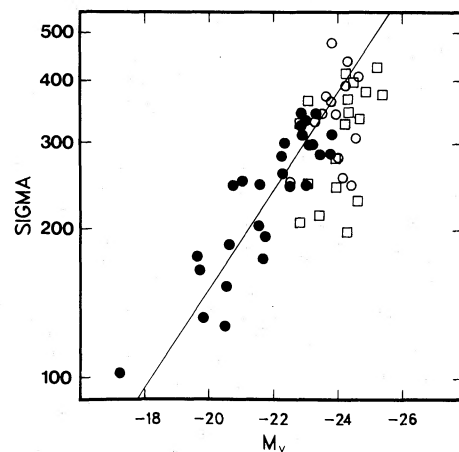


FIG. 5.—The log of the velocity dispersion versus absolute visual magnitude for elliptical galaxies (filled circles) and the BCM galaxies (open symbols). The line is the best fit of the  $L \propto \sigma^4$  relation to the E galaxies (see eq. [1]). The open squares are those BCM galaxies which are in the "Morgan cD" subset (see text), while the open circles are the other BCM galaxies. Most of the BCM galaxies are to the right of the line; that is, they are brighter than would be expected from their velocity dispersion and eq. (1).

TABLE 7  
STRUCTURAL PARAMETERS

Cluster	$\Delta L (10^{11} M_{\odot})$	$\beta$	$\alpha(16)$	Morgan cD?
A150	4.5	1.57	0.84	
A401	1.6	1.44	0.98	Y
A496	3.3	1.29	0.89	
A505	1.6	1.63	0.78	
A779	-0.8	1.62	0.61	
A994	-0.2	1.98	0.47	
A1177	2.5	1.37	0.65	
A1631	0.2	1.52	0.49	
A1904	...	1.65	0.77	
A2029	9.1	1.43	0.97	Y
A2052	4.3	1.22	0.95	Y
A2107	-1.7	1.54	0.80	
A2124	...	1.47	0.77	Y
A2147	4.3	1.54	0.75	
A2162	1.0	1.65	0.56	
A2199	4.3	1.62	0.85	Y
A2366	0.3	1.67	0.66	
A2457	-5.9	1.87	0.65	
A2589	2.2	1.32	0.82	Y
A2634	1.2	...	...	Y
A2666	-0.1	1.58	0.60	
A2670	5.1	1.56	0.85	Y
Virgo	-1.3	1.89	0.48	
MKW 2	-0.6	1.73	0.72	Y
MKW 4	2.7	1.51	0.74	Y
MKW 5	-1.5	1.64	0.57	Y
MKW 1s	0.9	1.64	0.58	Y
AWM 1	1.7	1.61	0.59	Y
AWM 2	0.8	1.65	0.44	Y
AWM 3	-0.8	1.71	0.35	Y
AWM 4	2.3	1.43	0.77	Y
AWM 5	5.7	1.54	0.72	Y
AWM 6	2.3	1.50	0.72	Y
AWM 7	4.3	1.05	0.93	Y

distribution of  $\Delta L$  in these clusters should resemble the distribution for E galaxies seen in Figure 7. On the other hand, if the statistical effects dominate (and mergers are irrelevant) then the BCM galaxies in these clusters should have a  $\Delta L$  distribution that resembles the simulation results.

### c) $\Delta L$ as a Measure of Dynamical Evolution

Another possible explanation for the  $\Delta L$  relation is the picture in which cD galaxies are the products of galaxy mergers in the centers of clusters of galaxies (OH; HO; Richstone and Malumuth 1983; Malumuth and Richstone 1984). A simple first approach (OH; HO) is that each merger results in a product which is homologous with the initial galaxies. Another picture of cD formation is that luminous material is stripped from cluster galaxies and forms an envelope around the central galaxy by gathering in the cluster potential well (Richstone 1975). We will not discuss this process in this paper, since the photometry here does not extend far enough out to measure the envelopes of many of the galaxies. As suggested by the results in Paper I, the models of Malumuth and Richstone (1984) confirm that the importance of stripping is strongly dependent on the cluster richness. Since very few of the clusters in this sample are richer than richness class 1, tidal stripping should not be very important for most of the galaxies here. The discussion in this paper is restricted to the merger models of cD formation.

In this model a BCM galaxy grows in luminosity with each merger, but its velocity dispersion remains unchanged (see Paper I; see also OH and HO). This model also predicts that

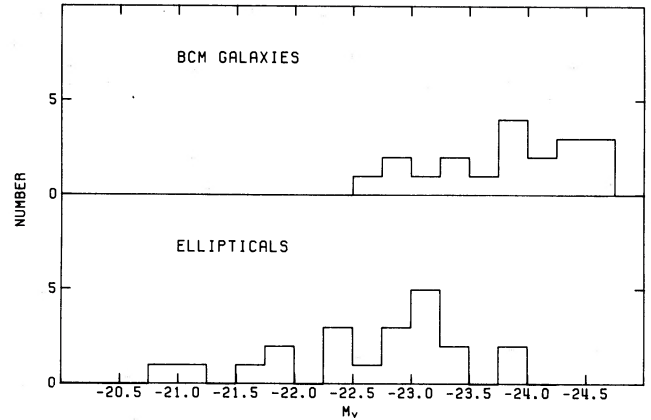


FIG. 6.—Histograms of the magnitudes of the elliptical galaxies and the BCM galaxies with velocity dispersions in the range  $193 \text{ km s}^{-1} \leq \sigma \leq 346 \text{ km s}^{-1}$ . The BCM galaxies average 1.22 mag brighter than the E galaxies in the range of velocity dispersions, even though the average velocity dispersions are almost the same ( $279 \text{ km s}^{-1}$  for the BCM galaxies and  $277 \text{ km s}^{-1}$  for the E galaxies).

the radius,  $R_e$ , and the logarithmic derivative of the luminosity,  $\alpha(16)$ , will increase, and the surface brightness will decrease with each merger (OH; HO). Here  $\alpha(16)$  is defined as  $[d(\ln L)/d(\ln R)]_{R=16 \text{ kpc}}$ . Since the velocity dispersion is constant in this model, the luminosity residual of a BCM galaxy in Figure 5 is an indication of how far the galaxy has evolved. In Paper I we saw that for the smaller sample  $R_e$  did increase and  $I_e$  did decrease with the  $M_{\sigma} - M_v$  residual in approximately the way predicted by homologous merger models. Here we will use the luminosity residual,  $\Delta L = L_v - L_{\sigma}$ , since an equal change in magnitude may represent a single merger for a small galaxy or several mergers (or one merger with a larger galaxy) for a large galaxy.

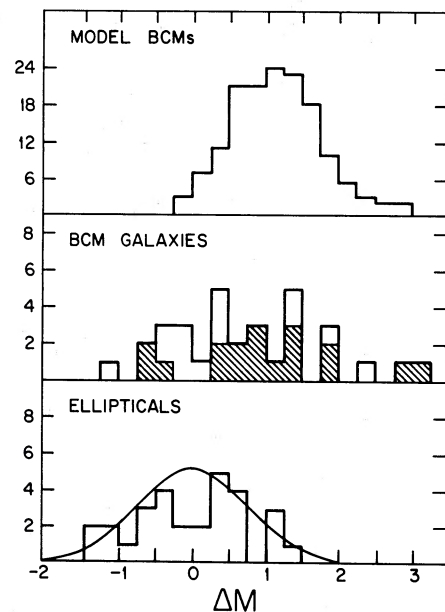


FIG. 7.—Histograms of the luminosity residuals from the  $L-\sigma$  relation for E galaxies and BCM galaxies. The residuals of the elliptical galaxies are small and symmetric about zero, while the BCM galaxies have mostly positive residuals, many of them quite large. The Morgan cD's are shown in hatched areas and have a distribution of residuals which are more positive and larger than the distribution of the BCM galaxies as a whole.

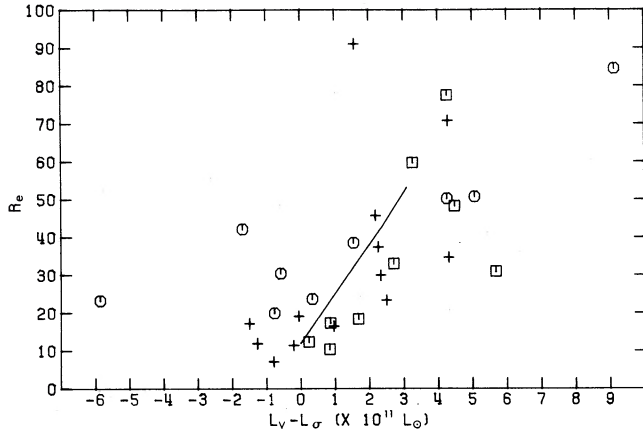


FIG. 8.—Effective radius,  $R_e$ , of the BCM galaxies versus the luminosity residual,  $L_v - L_\sigma$ , from the E galaxy  $L$ - $\sigma$  relation. The open squares are the BCM galaxies with  $\sigma < 250 \text{ km s}^{-1}$ , the open circles are BCM galaxies with  $250 \text{ km s}^{-1} < \sigma < 370 \text{ km s}^{-1}$ , and the plus signs are BCM galaxies with  $370 \text{ km s}^{-1} < \sigma < 370 \text{ km s}^{-1}$ . The line is from the homologous merger model of Paper I.

To test whether  $\Delta L$  measures the amount of dynamical evolution undergone by a BCM galaxy, we plot  $R_e$ ,  $I_e$ , and  $\alpha(16)$  against  $\Delta L$  in Figures 8, 9, and 10, respectively. The effective radius and surface brightness are used here, since they are less affected by seeing than are the core radius and central surface brightness. There is no significant trend of  $R_e$  with redshift for these galaxies, so seeing effects are not important in the determinations of  $R_e$ . The lines in Figures 8 and 9 are from the homologous merger model presented in Paper I. Since we derived the parameter  $\alpha(16)$  from the  $R^{1/4}$  law fits to the surface brightness profiles, there is no information in the data in Figure 10 that is not in Figure 8; it is included only for the purpose of comparison with the OH models. The line in Figure 10 is one of the models from OH's Figure 2, with  $L^*$  taken to be  $3.4 \times 10^{10} L_\odot$  ( $M_v^* = -21.5$ ; Schechter 1976). Although there is scatter in these plots, the data agree with the trends predicted by the homologous merger models. That is to say, BCM galaxies with large positive values of  $\Delta L$  are larger, with lower surface brightness and larger values of  $\alpha(16)$ , than galaxies with small values of  $\Delta L$ .

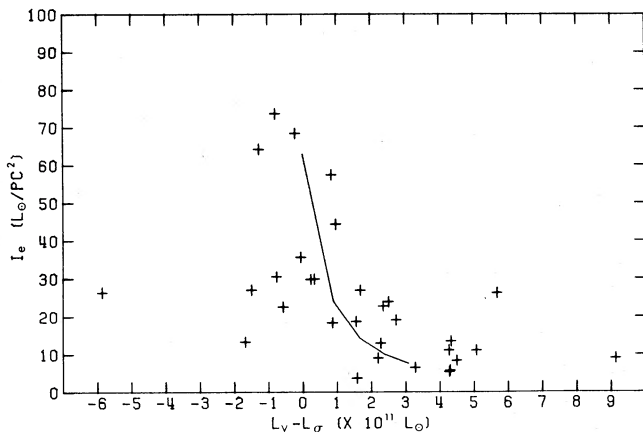


FIG. 9

It may appear at first that the scatter in Figures 8, 9, and 10 is uncomfortably large. However, a large amount of scatter is to be expected in these figures because the original (premerger) luminosity, radius, and surface brightness need not have been the same for each of the seed galaxies. If the velocity dispersion of a BCM galaxy is unchanged by mergers, then the BCM galaxies that we now see at different values of  $\sigma$  would have had a spread in luminosity from the start. It is clear that the radius of an elliptical galaxy increases with luminosity, although the slope of the relation is not well known (Kormendy 1977; Strom and Strom 1978; Davies *et al.* 1983; Schneider, Gunn, and Hoessel 1983), and unless  $R \propto L^{1/2}$ , we would also expect that the surface brightness is correlated with luminosity, since  $L \propto IR^2$ . We therefore expect that BCM galaxies with different values of  $\sigma$  started out with different luminosities, radii, and surface brightnesses. We examine below what would happen to the radius of a galaxy during a merger. From the virial theorem we have

$$\sigma_i^2 = K \frac{L_i}{R_i} \left( \frac{M}{L} \right)_i \quad (2a)$$

and

$$\sigma_f^2 = K \frac{L_f}{R_f} \left( \frac{M}{L} \right)_f \quad (2b)$$

for a galaxy before (subscripts  $i$ ) and after (subscript  $f$ ) a merger. We assume that in a merger  $\sigma$  and  $M/L$  remain the same. This may not be a good assumption, since, as we saw in Paper I,  $M/L$  in the core may increase during a merger. However, the important thing here is the value of  $M/L$  within the effective radius, which may vary much less in a merger. Rearranging and subtracting gives us

$$R_f = R_i + K \left( \frac{M}{L} \right) \frac{(L_f - L_i)}{\sigma^2}. \quad (3)$$

For equation (3) we see that galaxies of different initial sizes and values of  $\sigma$  will follow different tracks in Figure 8. BCM galaxies which are initially somewhat smaller will follow a track with a steeper slope because of their smaller  $\sigma$ , and will have a smaller intercept. BCM galaxies with velocity dispersions smaller than  $250 \text{ km s}^{-1}$  are plotted in Figure 8 as open

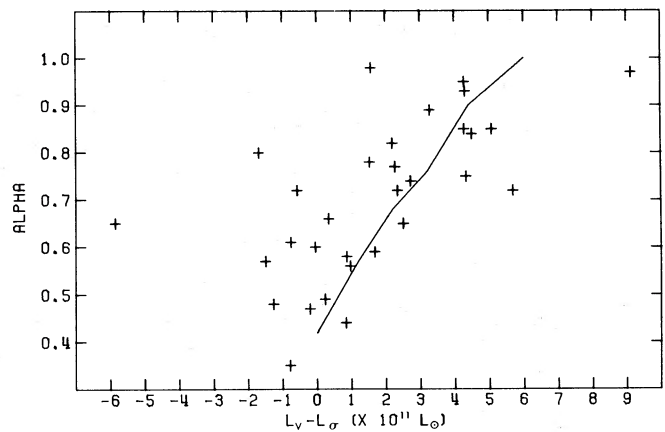


FIG. 10

FIG. 9.—Effective surface brightness versus the luminosity residual for the BCM galaxies. The line is from the homologous merger model of Paper I.

FIG. 10.—Logarithmic derivative of the luminosity at  $R = 16 \text{ kpc}$ ,  $\alpha(16)$ , versus the luminosity residual for the BCM galaxies. The line is from one of the Ostriker and Hausman (1977) homologous merger models.

squares, while BCM galaxies with  $\sigma > 370 \text{ km s}^{-1}$  are plotted as open circles. The other BCM galaxies are plotted as plus signs. It is clear that the lower  $\sigma$  galaxies do follow a relation with a steeper slope and a smaller intercept. From this we conclude that the scatter in Figure 8 is real and that it is what we would expect to arise from mergers, if the premerger galaxies did not start with the same effective radius.

#### d) The Shape of cD Galaxies

Schneider, Gunn, and Hoessel (1983, hereafter SGH) examined the photometric properties of the BCM galaxies compared with those of second- and third-ranked galaxies, with the use of these galaxies as cosmological probes in mind. They found from fits to the  $R^{1/4}$  law that there is a relation between  $R_e$  and  $I_e$  for BCM galaxies of the form

$$\log R_e = 1.103 + 0.315(I_e - 22),$$

where  $I_e$  is in units of mag arcsec $^{-2}$  and  $R_e$  is in kpc. They found similar relations for the second- and third-ranked galaxies. A least squares fit to the data in Table 5 gives a very similar relation:

$$\log R_e = 1.026 + 0.326(I_e - 22). \quad (4)$$

There is a slight shift of 0.20 mag at  $R_e = 30$  kpc between these two expressions. The shift is due mostly to the use of different colors (SGH use an  $r$  band, while we used a  $V$  band in this work).

A casual glance at the profiles in Figure 4 reveals that there is a considerable range of radii in each galaxy where the profile is approximately a power law. That is,  $I(r) \propto r^{-\beta}$ , where  $\beta$  is the power-law index. As mentioned earlier, some of the galaxies in this sample could not be fitted to King (1966) models because the surface brightness falls too slowly with radius. To quantify this we have fitted a power law to each profile in the range from  $4''$  to  $40''$ , except for M87 (NGC 4486), which was fitted from  $33''$  to  $470''$ . The values of  $\beta$  are given in Table 7 along with the logarithmic derivative of the luminosity,  $\alpha(16)$ . The mean value of  $\beta$  is  $1.56 \pm 0.03$  for this sample. This is considerably smaller than the mean of 1.82 for the SGH sample of BCM galaxies.

Examination of their Figure 6 (a histogram of  $\beta$ ) gives us one clue to the cause of this difference. The sample in this paper was selected against multiple nucleus galaxies (only A2634 and A2199 have more than one nucleus), while SGH's sample is 45% multiple nucleus galaxies. The six steepest (largest  $\beta$ ) profiles in their sample are all multiple nucleus galaxies. A comparison of the values of  $\beta$  in Table 7 with those of SGH shows that without the multiple nucleus galaxies the two distributions are similar at the small- $\beta$  end, but there are still more large- $\beta$  galaxies in the SGH sample. This suggests that another selection effect may be at work. The sample in this work is heavily weighted toward BCM galaxies classified as cD's or in clusters classified as Bautz-Morgan type I or type I-II, while the SGH sample was chosen to represent all Bautz-Morgan types. If the cD galaxies and the dominant galaxies which give rise to the Bautz-Morgan type I or type I-II clusters are the products of mergers, an interesting question arises. Could galaxies which have evolved by mergers have smaller values of  $\beta$ ?

To test this, we plot  $\beta$  against  $\Delta L$ , the parameter that measures growth through mergers, in Figure 11. There is a large scatter, but there is a tendency for the galaxies with small values of  $\beta$  to have large values of  $\Delta L$ . This may have two explanations within the context of the merger models of cD

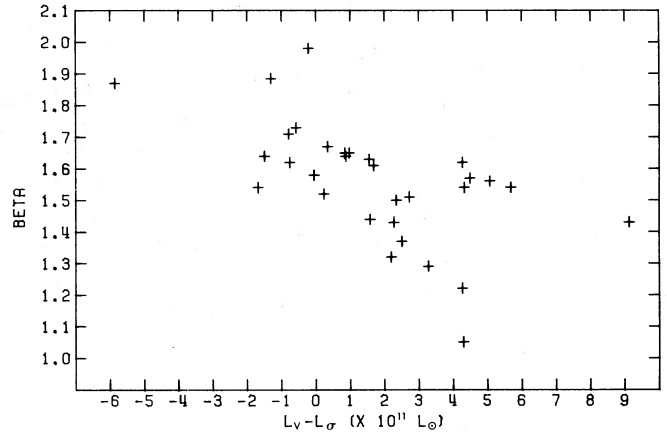


FIG. 11.—Index  $\beta$  of the power-law part of the surface brightness profile versus the luminosity residual for the BCM galaxies. The BCM galaxies with large positive residuals tend to have shallower power laws (smaller  $\beta$ ) than galaxies with residuals near zero.

galaxy formation. It may indicate that mergers are not strictly homologous. In that case the product of a merger is more extended (smaller  $\beta$ ) than the galaxies that merged to form it. If the central velocity dispersion does not change much, and the radius scales approximately as the luminosity in the merger, this may not be an important difference in the models. The more sophisticated models of Duncan, Farouki, and Shapiro (1983) have some of these characteristics without requiring homology. The other possibility is that galaxies with small  $\beta$  are more likely to merge with other galaxies than are galaxies with large  $\beta$ . This is reasonable, since galaxies with the same mass but larger radii will have a larger merger cross section.

A cD galaxy was originally defined as a supergiant galaxy with an "elliptical-like nucleus surrounded by an extensive envelope" (Matthews, Morgan, and Schmidt 1964). However, the greatly extended envelope detected by the photometry of O76 is much too faint to be seen by visual inspection on photographic plates (Oemler's "envelope" of A2670 starts at a surface brightness of about  $25 \text{ mag arcsec}^{-2}$ ; see Paper I). In that case, what property of the cD galaxies were Matthews, Morgan, and Schmidt (1964) referring to when they used the term "extensive envelope," since this is not the "envelope" in the O76 photometry?

We may be able to answer that question, since about half of the galaxies in this sample are classified as cD galaxies (18 of the 32 BCMs are Morgan cD's), and many of the others are in Bautz-Morgan type I or type I-II clusters. All but three of the galaxies in this sample have  $\beta$ -values much smaller than  $\beta = 2$ , the value of the Hubble law. Galaxies which have small values of  $\beta$  are more extended than ordinary ellipticals. We suggest that Morgan's term "extended envelope" refers to the appearance of a galaxy with a small value of  $\beta$ . Note that the large range of  $\beta$ -values found for brightest cluster members makes these galaxies a poor choice for cosmological tests which assume that all BCM galaxies have the same shape.

#### e) Mass-to-Light-Ratios

In Paper I we determined mass-to-light ratios in the cores of eight elliptical galaxies and seven BCM galaxies, using the method of King and Minkowski (1972). This method uses a fit of a King (1966) model to the surface brightness profile to estimate the central luminosity density. The core radius and

velocity dispersion then fix the central mass density. The core mass-to-light ratio is then just the ratio of the central mass density to the central luminosity density. When we applied this method to the galaxies in Paper I, we found that the BCM galaxies had a larger core mass-to-light ratio in  $V$  than the E galaxies ( $9.9 \pm 0.8$  and  $6.5 \pm 0.7$ , respectively). There was also a slight indication that the mass-to-light ratio of the BCM galaxies increased with the residual from the  $L \propto \sigma^4$  relation.

The derived values for  $M/L_v$  are listed in Table 5 for the 25 BCM galaxies fitted by a King (1966) model. We find for this larger sample that the average core mass-to-light ratio is  $9.0 \pm 0.8$ . This is consistent with our earlier result and significantly larger than the  $6.5 \pm 0.7$  average of the eight elliptical galaxies (see Paper I).

#### V. SUMMARY

To test the results of Paper I with a larger sample, velocity dispersions were obtained for a total of 46 brightest cluster member galaxies. In addition, surface photometry was done for 27 brightest cluster members, all but two of which have measured velocity dispersions. Using surface photometry from O76 and TR and the velocity dispersion of A2029 from Dressler (1979), we have a sample of 31 BCM galaxies with both velocity dispersions and surface photometry.

We find that many of the BCM galaxies are substantially brighter than would be predicted from their velocity dispersions and the best fitting  $L \propto \sigma^4$  relation for E galaxies. Twenty-three of the 31 BCM galaxies have positive residuals in luminosity, 14 of which have  $\Delta L \geq 2 \times 10^{11} L_\odot$ . It would be possible to reduce the size of these residuals and the discrepancy between positive and negative residuals by fitting a relation with a steeper slope than  $L \propto \sigma^4$ . However, where there is overlap between the E galaxies and the BCM galaxies in velocity dispersion, the BCM galaxies average 1.22 mag brighter.

We explored a selection model in which BCM galaxies are regarded as the brightest galaxies given a distribution of  $M$  at a given  $\sigma$ . Although this model does produce a large number of BCM galaxies with positive  $\Delta L$ , the shape of the distribution is not a good match to our sample. The match can be made better if there is a Malmquist bias of about 0.4 mag present in the elliptical galaxy sample. A better understood sample of elliptical galaxies is necessary to test this model. However, a more stringent test may be to repeat the measurements made in

this paper with a sample of BCM galaxies in Bautz-Morgan type III and type II-III clusters.

Simple homologous merger models of cD galaxy formation such as those of OH and HO predict that the velocity dispersion of the product of a merger will be about the same as the initial galaxy. The luminosity grows, while the velocity dispersion stays the same. These simple models also predict that the radius and the logarithmic derivative of the luminosity will also become larger, while the surface brightness will decrease. Our data show that the BCM galaxies with the largest luminosity residuals from the  $L$ - $\sigma$  relation for E galaxies have the largest effective radii and logarithmic derivatives of the luminosity,  $\alpha(16)$ , and the lowest surface brightnesses. We have also shown that the index of the power-law part of the surface brightness profile is correlated with the luminosity residual,  $\Delta L$ , in the sense that galaxies with large  $\Delta L$  have profiles which are flatter. This may have been the basis of the initial cD classification.

The core mass-to-light ratios of this larger sample are significantly larger than those of E galaxies; however,  $M/L$  does not correlate with  $\Delta L$  or with  $L$ .

Overall, the larger sample of BCM galaxies in this paper confirms the trends found in Paper I. We find that the data are for the most part consistent with simple merger models for cD galaxy formation. However, since the BCM galaxies which have the largest excess luminosities are the flattest, mergers may not be homologous.

We would like to thank Dr. Donald York for making the Princeton University CCD camera available to us. We are also grateful to Drs. Dennis Hegyi and Donald Gudehus for their help with the reduction of the photometry data. In addition, we are grateful to the support staff of Kitt Peak National Observatory for their help in the acquisition and preliminary reductions of some of the photometry data. We would also like to thank Dr. Matt Johns for his help with the equipment at the McGraw-Hill Observatory, Drs. Brad Whitmore, Paul Schechter, and Brian Flannery for developing some of the computer programs used in this work, and Dr. Douglas Richstone for many useful discussions. The suggestion of the referee led to the investigation of selection as a possible source of the  $\Delta L$  distribution. This research was supported by the NSF through grant AST 8202930.

#### REFERENCES

- Abell, G. O. 1958, *Ap. J. Suppl.*, **3**, 211.  
 Albert, C., White, R. and Morgan, W. 1977, *Ap. J.*, **211**, 309 (AWM).  
 Bahcall, N. A. 1980, *Ap. J. (Letters)*, **238**, L117.  
 Bautz, L. O., and Morgan, W. W. 1970, *Ap. J. (Letters)*, **162**, L149.  
 Davies, R. L. 1981, *M.N.R.A.S.*, **194**, 879 (D81).  
 Davies, R. L., Efstathiou, G., Fall, S. M., Illingworth, G., and Schechter, P. L. 1983, *Ap. J.*, **266**, 41.  
 de Vaucouleurs, G. 1958, in *Handbuch der Physik*, Vol. **53**, ed. S. Flügge (Berlin: Springer-Verlag), p. 311.  
 de Vaucouleurs, G., and Capaccioli, M. 1979, *Ap. J. Suppl.*, **40**, 699.  
 de Vaucouleurs, G., de Vaucouleurs, A., and Corwin, H. G. 1976, *Second Reference Catalogue of Bright Galaxies* (Austin: University of Texas Press) (RC2).  
 Dressler, A. 1978, *Ap. J.*, **223**, 765.  
 ———, 1979, *Ap. J.*, **231**, 659.  
 Duncan, M. J., Farouki, R. T., and Shapiro, S. L. 1983, *Ap. J.*, **271**, 22.  
 Faber, S. M., Burstein, D., and Dressler, A. 1977, *A.J.*, **82**, 941 (FBD).  
 Faber, S. M., and Jackson, R. E. 1976, *Ap. J.*, **204**, 688 (FJ).  
 Geller, M. J., and Peebles, P. J. E. 1976, *Ap. J.*, **206**, 939.  
 Gunn, J. E., and Oke, J. B. 1975, *Ap. J.*, **195**, 255.  
 Hausman, M. A., and Ostriker, J. P. 1978, *Ap. J.*, **224**, 320 (HO).  
 Hegyi, D., Gudehus, D., and Sharkin, S. 1983, private communication.  
 Hubble, E. P. 1930, *Ap. J.*, **71**, 231.  
 Kent, S. M. 1983, *Ap. J.*, **266**, 562.  
 King, I. R. 1966, *A.J.*, **71**, 64.  
 King, I. R., and Minkowski, R. 1972, in *IAU Symposium 44, External Galaxies and Quasi-Stellar Objects*, ed. D. S. Evans (Dordrecht: Reidel), p. 87.  
 Kormendy, J. 1977, *Ap. J.*, **218**, 333.  
 Leir, A. A., and van den Bergh, S. 1977, *Ap. J. Suppl.*, **34**, 381.  
 Malumuth, E. M., and Kirshner, R. P. 1981, *Ap. J.*, **251**, 508 (Paper I).  
 Malumuth, E. M., and Richstone, D. O. 1984, *Ap. J.*, **276**, 413.  
 Matthews, T. A., Morgan, W. W., and Schmidt, M. 1964, *Ap. J.*, **140**, 35.  
 Morgan, W. W., Kayser, S., and White, R. A. 1975, *Ap. J.*, **199**, 545 (MKW).  
 Morgan, W. W., and Lesh, J. R. 1965, *Ap. J.*, **142**, 1364.  
 Oemler, A. 1976, *Ap. J.*, **209**, 693 (O76).  
 Ostriker, J. P., and Hausman, M. A. 1977, *Ap. J. (Letters)*, **217**, L125 (OH).  
 Peach, J. V. 1969, *Nature*, **223**, 1140.  
 Peebles, P. J. E. 1968, *Ap. J.*, **153**, 13.  
 Pence, W. 1976, *Ap. J.*, **203**, 39.  
 Richstone, D. O. 1975, *Ap. J.*, **200**, 535.  
 Richstone, D. O., and Malumuth, E. M. 1983, *Ap. J.*, **268**, 30.  
 Sandage, A. R. 1973, *Ap. J.*, **183**, 711.  
 ———, 1976, *Ap. J.*, **205**, 6.  
 Sandage, A. R., and Hardy, E. 1973, *Ap. J.*, **183**, 743.  
 Sandage, A. R., Kristian, J., and Westphal, J. A. 1976, *Ap. J.*, **205**, 688.  
 Sargent, W. L. W., Schechter, P. L., Boksenberg, A., and Shorridge, K. 1977, *Ap. J.*, **212**, 326 (SSBS).  
 Schechter, P. L. 1976, *Ap. J.*, **203**, 297.

- Schechter, P. L. 1980, *A.J.*, **85**, 801 (S80).  
Schechter, P. L., and Gunn, J. E. 1979, *Ap. J.*, **229**, 472.  
Schneider, D. P., Gunn, J. E., and Hoessel, J. G. 1983, *Ap. J.*, **268**, 476 (SGH).  
Schweizer, F. 1979, *Ap. J.*, **233**, 23.  
Schild, R., and Davis, M. 1979, *A.J.*, **84**, 311.  
Strom, S. E., and Strom, K. M. 1978, *Ap. J. (Letters)*, **225**, L93.  
Thuan, T. X., and Romanishin, W. 1981, *Ap. J.*, **248**, 439 (TR).
- Tonry, J. L. 1980, Ph.D. thesis, Harvard University (T80).  
Tremaine, S. D., and Richstone, D. O. 1977, *Ap. J.*, **212**, 311.  
Whitmore, B. C., and Kirshner, R. P. 1981, *Ap. J.*, **250**, 43 (WK).  
Whitmore, B. C., Kirshner, R. P., and Schechter, P. L. 1979, *Ap. J.*, **234**, 68.  
Young, P. J., Sargent, W. L. W., Kristian, J., and Westphal, J. A. 1979, *Ap. J.*, **234**, 76.

ELIOT M. MALUMUTH: Department of Physics, Rutgers University, Piscataway, NJ 08854

ROBERT P. KIRSHNER: Department of Astronomy, University of Michigan, Ann Arbor, MI 48109